UiT The Arctic University of Norway

Faculty of Health Sciences, Department of Pharmacy

Microbial Pharmacology and Population Biology (MicroPop)

The effect of β-lactamase evolution on biofilm formation in *Vibrio cholerae*

Anne Sofie Bernhardsen Haukefer

Supervisor: Christopher Fröhlich, PhD

Co-supervisor: Øyvind Myrvoll Lorentzen, MD

Thesis for the degree Master of Pharmacy, FAR-3911, May 2023

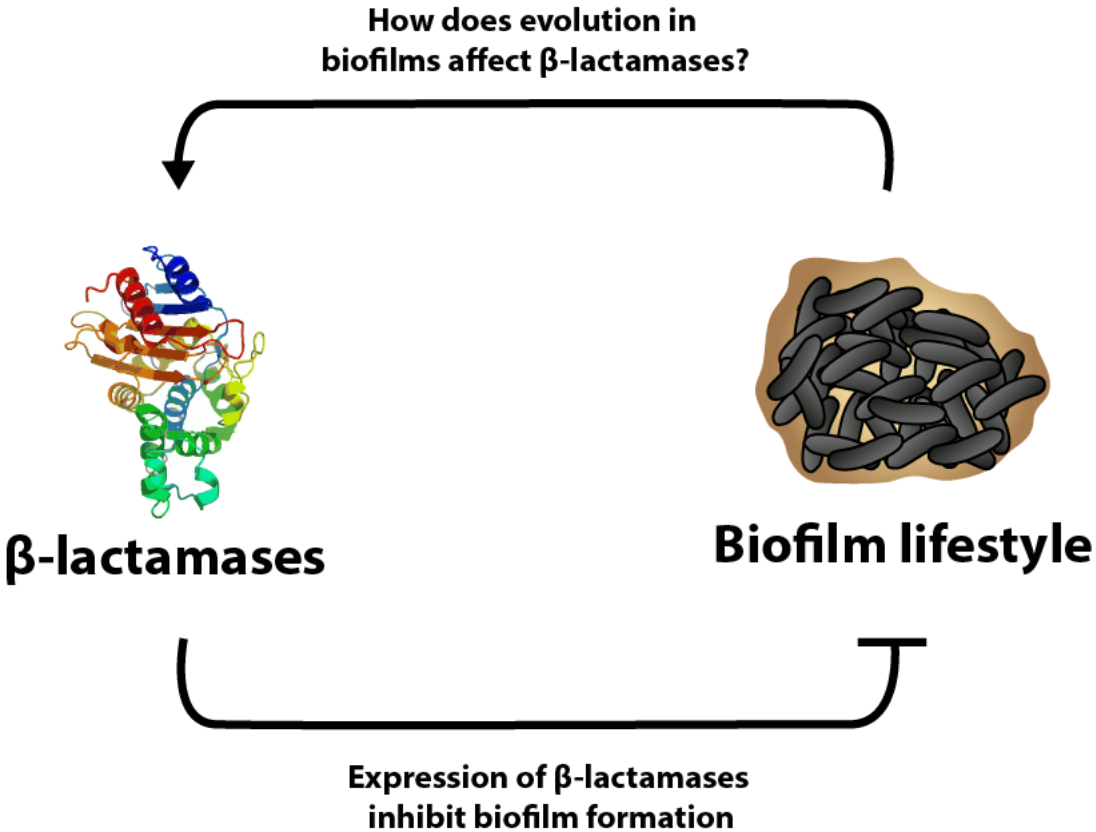

Acknowledgments

This master project was performed at the Microbial Pharmacology and Population Biology Research Group (MicroPop), at the Department of Pharmacy, UiT – The Arctic University of Norway in the period August 2022 – May 2023. I would like to express my sincere thanks to all members of the MicroPop group. Thank you for all your guidance and support, and for including me in your research group.

I would like to express my deepest gratitude to my supervisors, Christopher Fröhlich and Øyvind Myrvoll Lorentzen. Thank you for providing invaluable direction throughout my master's thesis and being there for me whenever I needed help. Your expertise and patience have been invaluable to me and crucial to the success of this thesis.

I would also like to thank Rebekka Rolfsnes for always taking the time to help. Thank you for everything you taught me in the lab and for always ensuring me that no questions are too dumb.

A special thanks to fellow student Gøril Laugsand. Thank you for all time we spent together, filled with laughter, positivity, frustration, and so much more. This year would not have been the same without it!

Lastly, I would like to thank my family. Your endless support, love, and understanding have been worth more than I can express on paper.

Anne Sofie Bernhardsen Haukefer, May 2023

Abstract

Antimicrobial resistance (AMR) has emerged as one of the greatest threats to public health in the 21st century. Especially, the production of β-lactamase enzymes has become the leading cause of β-lactam resistance in Gram-negative pathogens. In addition, many of the pathogens associated with extensive antimicrobial resistance form biofilms, which further increases their persistence. Studies from different Gram-negative bacteria have demonstrated that β-lactamases can inhibit biofilm formation. However, no study has investigated how the biofilm lifestyle affect β-lactamase evolution. Thus, acquiring insights into the evolutionary relationship between biofilms and β-lactamases could generate knowledge that has implications for combating AMR. Using a biofilm quantification assay, directed evolution based on mutational libraries, and biofilm evolution, this master project aimed to understand how the production and evolution of β-lactamases affect biofilm formation in *V. cholerae.* Quantification of biofilm formation demonstrated that 7/8 tested β-lactamases inhibited biofilm formation in *V. cholerae*. Applying strong biofilm selection on a mutational library of the β-lactamase KPC-2 identified multiple KPC-2-harboring mutants with increased biofilm formation. Sequencing of the evolved mutants revealed the presence of single and double mutants sharing an amino acid change at the same position (N136x). Functional studies of the newly evolved variants, using a binding-deficient mutant (S70A), revealed that disruption of binding (S70A) led to reversal of the observed increase in biofilm formation. Thus, suggesting that the evolutionary changes in the KPC-2 mutants could be related to the evolution of a new enzymatic function rather than a loss-of-function. Taken together, this study shows that the evolution of β-lactamases and biofilms affect each other. Comprehending evolutionary connections, as described in this study between biofilm and the evolution of $bla_{\text{KPC-2}}$ in *V. cholerae*, may help to understand the spread and evolution of antimicrobial resistance genes.

List of abbreviations

AMR	Antimicrobial resistance
bla	Gene that encodes β-lactamase
CMY	Cephamycinase
CTX-M	Cefotaximase (CTX) from Munich (M)
CV	Crystal Violet
dH_2O	Distilled water
DNA	Deoxyribonucleic acid
EtOH	Ethanol
ESBLs	Extended-spectrum β-lactamases
KPC	*Klebsiella pneumonia* carbapenemase
LB	Lysogeny Broth
MBLs	Metallo-β-lactamases
MIC	Minimum Inhibitory Concentration
NDM	New Delhi metallo-β-lactamase
OD	Optical density
OXA	Oxacillinase
PBPs	Penicillin-binding proteins
PBS	Phosphate buffered saline
PCR	Polymerase chain reaction
PG	Peptidoglycan
RNA	Ribonucleic acid
Rpm	Rotation per minute
SBLs	Serine β-lactamases
SD	Standard deviation
SEM	Standard error of the mean
TEM	Named after the patient (Temoneira)
VIM	Verona integron-encoded metallo-β-lactamase

Table of Contents

1 INTRODUCTION

1.1 Antimicrobial resistance (AMR)

1.1.1 Antimicrobials

Sir Alexander Fleming's coincidental discovery of penicillin in 1928 completely revolutionized the world of medicine and started what is called the golden era of antibiotics (1). Antibiotics are medications used to treat or prevent infections caused by bacteria. They act by either killing the bacterial cells (bactericidal) or suppressing their growth (bacteriostatic). The discovery of antibiotics has led to diseases earlier considered life-threatening with high mortalities, such as bloodstream infections, pneumonia, and pyelonephritis, becoming treatable (2). As well as in treating infectious diseases, antibiotics have also made several medical procedures feasible through perioperative antibiotic prophylaxis, making antibiotics a cornerstone in modern medicine which has saved millions of lives to this day (1).

1.1.2 Resistance mechanisms against antimicrobials

It was in the golden era, between the 1940s and 1960s, the majority of today's used antibiotics were discovered. However, since then the discovery of new antibiotics has declined drastically, in line with the evolution of antibiotic resistance becoming an inclining concern (1). The possibility of bacteria developing resistance mechanisms was early on called attention to, and as early as 1945 Fleming cautioned against misuse of the drug leading to bacterial resistance (3).

Table 1.1 provides a comprehensive overview of major classes of antibiotics and their resistance mechanisms. Generally, there are four main mechanisms involved in resistance development (4):

1. Reduction in intracellular drug accumulation. This mechanism involves reducing the amount of antibiotic that can enter the bacterial cell, either by reducing the permeability of the cell membrane or by actively removing the antibiotic using efflux pumps. The outer membrane found in Gram-negative bacteria acts as a barrier to antibiotics which reduces their ability to penetrate the cell.
2. Modification or alteration of the bacterial antibiotic target. Bacteria can modify the structure of the target protein that the antibiotic binds to, which in turn leads to the target being less susceptible to the antibiotic.
3. Inactivation and modification of the drug. Bacteria can also produce enzymes that alter the antibiotic molecule itself, leaving it inactive. β-lactamases are examples of such enzymes.
4. Target bypass (bypass of whole metabolic pathways). This mechanism involves creating an alternative pathway that bypasses the antibiotic by rendering the original target redundant. This can occur when an additional gene is acquired that can confer the required properties to the cell but is not effectively suppressed by the original antibiotic.

Table 1.1. Overview of major classes of antibiotics, their mechanisms of action, drug targets, and resistance mechanisms (4). The mechanisms of resistance are marked as followed; 1 = altered uptake. 2 = target modification. 3 = drug modification. 4 = target bypass

Mechanism of action	Antibiotic class	Drug target	Mechanism of resistance
Inhibition of cell wall synthesis	β-lactams	Penicillin-binding proteins	1, 2, 3, 4
	Glycopeptides	Terminal D-Ala-D-Ala	2, 4
Disruption of cell wall integrity	Lipopeptides	Outer cell wall	2
	Cationic peptides	Outer cell wall	2
Inhibition of protein synthesis	Aminoglycosides	30S ribosomal unit	1, 2, 3
	Tetracyclines	30S ribosomal unit	1, 2, 3, 4
	Macrolides	23S RNA in 50S ribosomal unit	1, 2, 3
	Lincosamides	50S ribosomal unit	1, 2, 3
	Streptogramins	23S RNA in 50S ribosomal unit	1, 2, 3
	Oxazolidinones	23S RNA in 50S ribosomal unit	2
	Phenicols (chloramphenicol)	50S ribosomal unit	1, 2, 3
Inhibition of folic acid synthesis	Sulfonamides	Dihydropteroate synthetase	1, 2, 4
	Pyrimidines (trimethoprim)	Dihydrofolate reductase	1, 2, 4
Inhibition of DNA synthesis	Fluoroquinolones	DNA gyrase	1, 2
Inhibition of RNA synthesis	Rifampin	RNA polymerase	2, 3

Gram-negative bacteria can prevent antibiotics from entering the cell, which can be explained by the structural differences in bacteria. Based on the chemical and physical properties of their cell walls, bacteria are classified as either Gram-positive or Gram-negative. Bacterial cell walls are made up of peptidoglycan (PG), a highly cross-linked polymer that confers physical strength and rigidity to bacteria (5). Gram-positive bacteria have a thick cell wall consisting of several layers of PG, whereas Gram-negative bacteria have only a thin cell wall but in difference to Gram-positive bacteria, have an additional outer membrane (Figure 1.1)

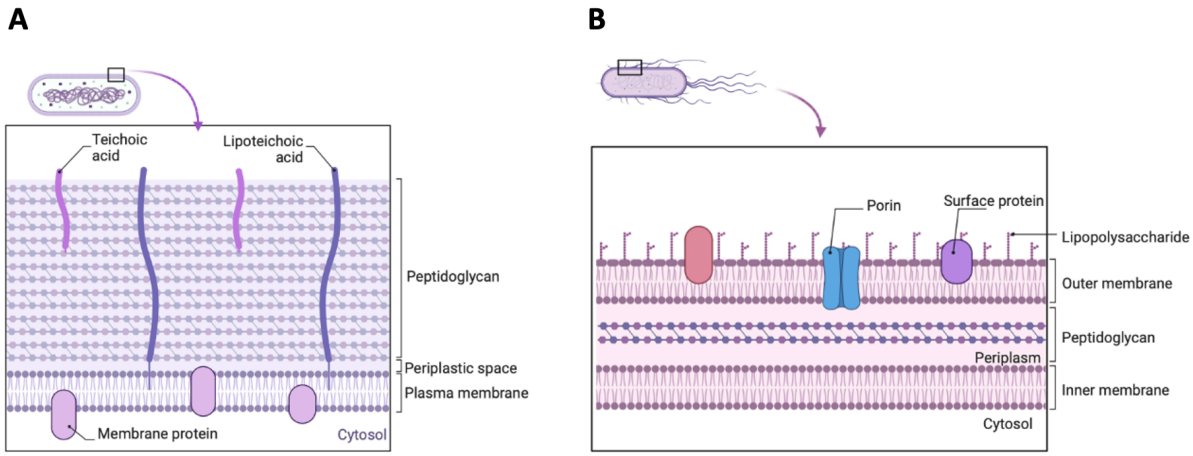

Figure 1.1. (A) Gram-positive bacteria cell wall structure. **(B)** Gram-negative bacteria cell wall structure. Figure created in Biorender.com.

Antimicrobial resistance can be either intrinsic, in which bacteria are naturally resistant to certain antibiotics, or acquired, where new resistance mechanisms are obtained through either gene mutations or by transfer of genetic material between bacteria (4). For instance, the main cause of intrinsic resistance of Gram-negative pathogens is due to their outer membrane, as previously noted, which simply prevents drugs from entering the cell, and thus, not reaching their target site (4). One way acquired resistance can be achieved is through horizontal gene transfer of foreign DNA harboring antimicrobial resistance genes. Mobile genetic elements, such as plasmids (extrachromosomal genetic material), transposons ("jumping genes"), and bacteriophages (bacteria-infecting viruses) enable horizontal gene transfer between organisms. These elements are transferred between bacteria through three main mechanisms (6):

1. Transformation, in which bacteria take up free fragments of DNA, often plasmids, from the environment.
2. Transduction, in which DNA is transferred via a bacteriophage from one cell to another.
3. Conjugation, in which bacteria directly transfer genetic material, e.g., plasmids, to another bacterial cell.

1.1.3 β-lactamases as the main source of β-lactam resistance

β-lactam antibiotics belong to the most prescribed class of antibiotics with numerous clinical indications including pneumonia, pyelonephritis, sepsis, and soft tissue infections (7). They are grouped together based on a shared structural feature, the β-lactam ring, and sub-classified into four major groups: penicillins, cephalosporins, carbapenems, and monobactam (7). They exhibit bactericidal effects by targeting penicillin-binding proteins (PBPs), which are the proteins responsible for the synthesis/crosslinking of PG (8). By resembling the terminal D-Ala-D-Ala peptide sequence, the natural substrate of PBPs, β-lactams binds to PBPs and inactivates them, which ultimately leads to bacterial cell lysis (5).

Extensive use of these drugs has selected for several resistance mechanisms (Table 1.1), including expression of β-lactamase enzymes. In general, enzymes are biological catalysts that speed up chemical reactions in living organisms. Enzymes produced by bacteria are involved in a variety of antibiotic resistance mechanisms by lowering a reaction's activation energy necessary to transform a reactant into a product. The most threatening and frequent mechanism of antibiotic resistance in Gram-negative bacteria is represented by the production of β-lactamase, enzymes catalyzing the hydrolysis of the crucial β-lactam ring, thereby inactivating β-lactam antibiotics (9). The molecular classification system is based on their amino acid sequences and divides the enzymes into four classes known as the Ambler classification (8), including the serine β-lactamases (SBLs; classes A, C, and D) and the metallo-β-lactamases (MBLs; class B). Besides the Ambler classification, which is based on sequence identity, the Bush-Jacobi-Medeiros system is another classification system in use today which sub-divides the β-lactamases according to functionality (10-12).

In this system, β-lactamases are classified into three groups depending on β-lactam substrate degradation, and on the inactivation properties of β-lactamase inhibitors such as clavulanic acid, tazobactam, and sulbactam. This system includes cephalosporinases in group 1; broad-spectrum, inhibitor-resistant, and extended-spectrum β-lactamases and serine carbapenemases in group 2; and metallo-β-lactamases in group 3. Each of the three groups is again divided into several subgroups. The system was first proposed in 1989 (10) and has been expanded and updated two times since then, due to the discovery of new β-lactamases. The β-lactamases included in this study span all three of the functional groups. Enzymes in functional group 1 are cephalosporinases from molecular class C, including CMY-2.

Functional group 2 represents the largest group of β-lactamases, including molecular classes A and D, and is mainly due to an increasing number of ESBLs being identified (11). ESBLs are extended-spectrum β-lactamases that are resistant to several antibiotic classes including third-generation cephalosporins. KPC-2, TEM-1, CTX-M-15, OXA-48, and OXA-163 belong to this group. KPC-2 is a carbapenemase. MBLs represent functional group 3 and include VIM-2 and NDM-1 (11).

Reaction mechanism of SBLs and MBLs

While SBLs utilize an active site serine amino acid residue for the nucleophilic attack of the β-lactam ring, MBLs utilize a metal-activated water nucleophile to drive the hydrolysis (13). The same general two-domain (α and α/β) fold is found in all SBLs; however, the amino acid sequence identity varies significantly between the classes (as low as 15% sequence identity in some cases). Despite the great diversity in amino acid sequence, the active-site residues involved in hydrolysis are almost entirely conserved (including the SBL S-x-x-K motif) (14). The three classes of SBLs all catalyze the hydrolysis of β-lactams through two steps: acylation and deacylation. First, a non-covalent enzyme-substrate complex is formed between the drug and the enzyme. The nucleophilic serine is activated by a strategically positioned general base and attacks the carbonyl carbon of the scissile β-lactam amide bond to produce the acyl-enzyme intermediate via a tetrahedral oxyanion transition state. Subsequently, the general base activates an incoming deacylating water molecule in order to hydrolyze the acyl-enzyme and release the degradation product. The hydrolysis mechanism of the SBLs shares similarities across the Ambler classes A, C, and D but differ regarding the identities of the necessary general base and the precise interactions made by them (13). For example, within class A β-lactamases E166 has been established as a key active-site residue, by activating the deacylating water which facilitates the termination of the β-lactam from the acyl-enzyme complex (15). In class C β-lactamases, Y150 serves as the general base, whereas carboxylated lysine (K73) serves as the general base in class D (Figure 1.2). The MBL superfamily consists of many members, that show great divergence in both sequence and function (16). Relative to SBLs, MBLs follow a different hydrolysis mechanism as they hydrolyze the scissile amide bond of β-lactams by using the OH group from a water molecule that is coordinated by Zn^{2+} (Figure 1.2) (17). Most MBLs are able to hydrolyze nearly all β-lactams, apart from monobactams (monocyclic β-lactams), giving them an extremely broad substrate spectrum (18).

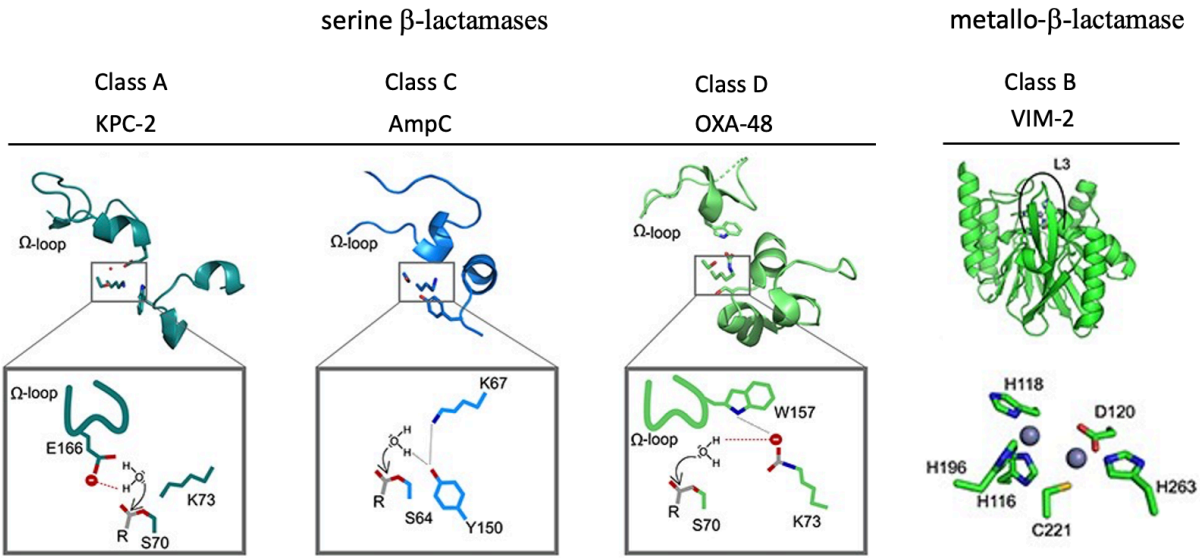

Figure 1.2. Showing active site residues of Ambler classes A, B, C, and D. Figure adapted with permission from (18).

β-lactam resistance in Gram-negative bacteria poses a major health concern. Firstly, due to the intrinsic resistance as outlined earlier which is attributed to the outer membrane in Gram-negative bacteria (Figure 1.1B). Secondly, *bla*-genes are frequently located on transferable plasmids that readily can spread among bacteria through horizontal gene transfer (19). This health concern is also reflected in the priority pathogen list by The World Health Organization (WHO) (20). WHO has identified a list of priority pathogens that pose the greatest threat to human health due to their resistance to multiple antibiotics. Based on the urgency and need for new antibiotics, the list is divided into three categories: medium, high, and critical priority pathogens. The three species identified as critical priority pathogens by WHO are carbapenem-resistant *Acinetobacter baumannii*, carbapenem-resistant *Pseudomonas aeruginosa*, and carbapenem-resistant and ESBL-producing *Enterobacteriaceae*, including the strains *Klebsiella pneumoniae* and *Escherichia coli* (20). These are the most critical and are all Gram-negative bacteria that are associated with β-lactamase resistance.

1.1.4 Evolution of new functions in β-lactamases

Natural evolution is the process by which organisms change over time due to environmental pressures, such as changes in climate, predation, or food availability (21). Through accumulation of random mutations and selection of beneficial mutations in a specific environment, this process may result in new traits increasing the organism's chance of survival (21). β-lactamases are ancient enzymes that due to an evolutionary pressure, have naturally evolved over several years resulting in the selection of enzymes able to hydrolyze β-lactams (22). SBLs have been shown to be evolutionarily related to PBPs. MBLs are related to another source, however, their evolutionary roots remain more elusive (22). The examples from natural evolution demonstrate that these enzymes can possess multifunctionality and that these functions can be selected for and evolve when the selection pressure changes.

Directed evolution is a laboratory-based approach used to fast-forward the evolution process by introducing genetic variance in a gene. This approach can be used to create both random mutations (e.g., error-prone PCR) and specific mutations (e.g., site-directed mutagenesis) and is commonly used in biotechnology to investigate evolutionary relationships. Using directed evolution, a former study demonstrated how antibiotics can mediate the evolution of β-lactamases (23) and how other functional traits can be selected for (e.g. phosphotriesterase activity in MBL) (24). These studies have shown that structural changes in these enzymes, due to mutations acquired around and distant to the active site, can modulate the enzymatic activity by adapting the enzymatic cavity (16). In this master project, directed evolution will be utilized to explore the evolutionary connection between β-lactamase enzymes and biofilms.

1.2 Biofilm as a lifestyle

1.2.1 The basics of biofilms: Formation, Growth, and Survival

Biofilms are structured communities of bacteria attached to a surface or each other, encased by a self-produced, polymer matrix (25). Biofilm formation can occur on both abiotic and biotic surfaces, or as cells attach to each other. It is a complex multicellular behavior, involving several stages. Following initial attachment, extracellular matrix components are produced, microcolonies are formed, and lastly, highly organized, three-dimensional structures are developed (26). Biofilms represent one of the key survival strategies for bacteria and represent the most common mode of bacterial growth in nature (25). The protective biofilm matrix shields the bacteria from stressors and threats (e.g., antimicrobials and predators). Because of this, biofilm formation can increase the tolerance of bacteria against antimicrobials and is associated with chronic infections and treatment failure (27). However, biofilm formation can be a costly process, by which the production of extracellular matrix potentially can reduce the maximal growth rate relative to planktonic cells (28). Therefore, the process of forming biofilms is strictly regulated and depends on environmental, chemical, and mechano-physical signals to weigh the cost of biofilm formation against the protective advantages that biofilms provide (28). Biofilms can be divided into submerged (solid-liquid interface), colony (solid-air interface), or pellicles (liquid-air interface) varieties depending on the type of occupied surface (29). When living in biofilms, bacteria are subjected to a selection pressure for obtaining beneficial, survival traits due to the environmental conditions. Indeed, studies have demonstrated how bacteria can undergo phenotypic changes and acquire new traits (e.g. increased biofilm formation) when experimentally evolved in biofilms and under stressful conditions (30, 31).

1.2.2 *Vibrio cholerae* as a biofilm model

Vibrio cholerae is a Gram-negative bacterium and the causative agent of the diarrheal disease cholera. Over the past 200 years, several pandemics have occurred including recent major outbreaks in Haiti and Yemen (32). Annually, *V. cholerae* causes 3 to 5 million cases of cholera and is associated with 100 000-120 000 deaths (32). Infection is spread through contaminated food and water, particularly affecting areas with inadequate sanitation and

access to clean drinking water. The pathogen causes severe watery diarrhea and rapid dehydration, which can cause hypotonic shock and potentially be life-threatening if left untreated (26).

As an environmental pathogen, *V. cholerae* is a natural inhabitant of aqueous environments and does not depend on the human host for survival (33). When transmitted from the aquatic environment into the human host, *V. cholerae* first enters the stomach before it continues into the small intestine. Here, toxigenic strains of *V. cholerae* colonize the small intestine, where they multiply and produce the diarrhea-inducing cholera toxin (34). During infection, *V. cholerae* is shed in the stool of infected humans by which bacteria re-enter the aqueous environment and potentially infect new hosts (35).

Biofilm formation plays a key role in the life cycle of *V. cholerae* and is important for environmental persistence and survival, transmission into the human host, and dissemination to new hosts and back to the environment (26). In the environment, the pathogen must adapt to a variety of changing circumstances, including nutrient deficiency, temperature changes, and predatory activity (26). One of the strategies *V. cholerae* employs to overcome these challenges is biofilm formation. In addition, biofilm formation aid in the pathogen's transit through the acidic environment in the stomach, by providing physical protection from acid shock, thereby increasing the infectivity of *V. cholerae* (26). Biofilms have also been described in the human intestine (35). Further, biofilm-like aggregates of *V. cholerae* have been observed in the human stools of cholera patients. Indicating that it could also be important for survival as it re-enters its aquatic environment after exiting the human host. These aggregates of biofilm-grown cells are considered hyper-infectious as they disperse *in vivo*, thus providing a large infectious dose of the pathogen (32).

Biofilms produced by *V. cholerae* can either adhere to solid surfaces or develop as biofilm pellicles at the air-liquid interface. Since biofilm formation plays a crucial role in the life cycle of *V. cholerae* it is a well-suited model organism for biofilm research, which has been frequently used as a model for investigation biofilm formation (35). Thus, *V. cholerae* is used in this project to study the effect of β-lactamases on biofilm development (28, 35).

1.3 Effects of β-lactamases on biofilm formation

The effect β-lactamases have on biofilm formation and *vice versa*, particularly with respect to the evolution of these enzymes, is highly understudied. A former study found that strains of *Pseudomonas aeruginosa* carrying TEM-1 encoding vectors led to abnormalities in twitching motility, adhesion, and biofilm formation, without impacting growth rates (8). The same study also investigated the effect of TEM-1 encoding vectors in *E. coli* which also resulted in decreased adhesion and biofilm formation without affecting the growth rate. Indicating that this is a non-species-specific effect (8). The inhibitory effect on biofilm formation was proposed to be restricted to class A and class D SBLs, as the expression of OXA-3 (class D), but neither class B nor class C β-lactamases, impaired biofilm formation by *P. aeruginosa* and *E. coli.* Site-directed mutagenesis was used to establish whether TEM-1 *per se* or instead its enzymatic activity was of importance for the inhibition of biofilm formation. Active-site serine mutated to alanine resulted in no defect in adherence being observed. Thus, the study showed that the catalytic serine residue of TEM-1 was important for the biofilm inhibition phenotype and that loss of enzyme activity restored the wild-type biofilm phenotype. Site-directed mutagenesis was also performed to determine if OXA-3's enzymatic activity was required for its effects on biofilm formation. An S70A/T71A double mutant of OXA-3, surprisingly, continued to impair adherence similarly to the unmodified enzyme, despite it no longer conferring resistance to the β-lactam ampicillin (8).

Another study investigated the interaction between the expression of β-lactamases (SFO-1, OXA-10-like, OXA-24, and TEM-1) and the composition and/or structure of PG, followed by an investigation of how the changes they observed in PG influenced biofilm formation, using *E. coli* as the model organism (36). Changes in PG composition were seen for the strains harboring SFO-1, OXA-10-like, and OXA-24. The strain harboring TEM-1 was also included in the biofilm formation assay although no changes were observed in its PG composition. However, all tested strains (SFO-1, OXA-10-like, OXA-24, and TEM-1) produced less biofilm relative to the control strain.

Results from these two studies indicate that members of class A and class D β-lactamases inhibit biofilm formation in *E. coli* and *P. aeruginosa.* However, none of them investigated how the biofilm lifestyle affect β-lactamase evolution. In this study, I will investigate how eight different β-lactamases, spanning all Ambler classes, affect biofilm formation in the pathogen *V. cholerae*. In addition, I will investigate the evolutionary relationship between β-

lactamases and biofilms, specifically if biofilm selection can affect the evolution of β-lactamases.

2 AIMS AND HYPOTHESIS

Biofilm represents the most common bacteria lifestyle and is key to the life cycle of multiple bacterial pathogens (25). Among them are *V. cholerae*, a Gram-negative enteric pathogen, and causative agent of cholera. In the last decades, antimicrobial resistance has become an increasing public health challenge worldwide. Among the most problematic pathogens are extensive antimicrobial-resistant biofilm-associated Gram-negative pathogens. The production of β-lactamases is the most important mechanism for the development of β-lactam resistance in Gram-negative pathogens. (9). Interestingly, a few studies have demonstrated that β-lactamases possess the ability to inhibit biofilm formation in *P. aeruginosa* and *E. coli* (8, 36). However, the molecular origin behind this phenomenon remains elusive. In addition, knowledge of the evolutionary relationship between biofilm development and the expression and evolution of β-lactamases is absent. Compared to the published studies, this work will first employ *V. cholerae* as a model system to study the effect of a wide selection of potentially plasmid transferable β-lactamases (KPC-2, TEM-1, CTX-M-15, NDM-1, VIM-2, CMY-2, OXA-48, and OXA-163), covering all Ambler groups, on biofilm formation. Further, to gain insights into the relationship of β-lactamase-mediated biofilm perturbance, I studied how the evolution of a specific enzyme (KPC-2) affects the ability of *V. cholerae* to form biofilm and vice versa.

In this project, I aimed to address the following research questions:

- Are β-lactamases from all Ambler classes functional in *V. cholerae*? And thus, can *V. cholerae* serve as a model system to study β-lactamase mediated biofilm changes?
- Published results in *P. aeruginosa* and *E. coli* demonstrated that the production of certain β-lactamases inhibits biofilm formation. Thus, this master project addressed the question of whether the production of a wide range of different β-lactamases has a similar effect in *V. cholerae?*
- Next, I aimed to close a knowledge gap in the literature by investigating the evolutionary link between biofilm development and β-lactamase evolution: Is it possible to select for β-lactamase mutants with increased biofilm-forming capacity?
- Finally, I wanted to characterize the functionality of potential β-lactamase mutants and asked: Do biofilm-selected mutations alter the functionality of these enzymes or will mutations simply inactivate the enzymes?

3 MATERIALS AND METHODS

3.1 Bacterial strains, media, and growth conditions

All strains and primers used and constructed within this study are shown in Appendix A (Table A1 and Table A2). Throughout the study, *Vibrio cholerae* C6706 was used as the model organism (37). *Escherichia coli* E.cloni® 10G was used for genetic manipulations (Lucigen). Unless otherwise noted, strains were cultured in Lysogeny-Broth (LB) media (10g/L of tryptone, 10 g/L of sodium chloride, and 5 g/L of yeast extract) with shaking (700 rpm), or on LB agar plates, at 37 °C. Unless otherwise stated, all strains harboring vectors were always cultured in, or plated on, media supplemented with chloramphenicol (Sigma-Aldrich) at the following final concentrations: 5 mg/L for *V. cholerae* and 25 mg/L for *E. coli*.

3.2 Molecular methods: general description

3.2.1 Polymerase Chain Reaction (PCR)

Polymerase chain reaction (PCR) is a standard *in vitro* technique used to rapidly amplify millions of copies of a specific gene of interest. Through repeating cycles of denaturation, annealing, and synthesis, this technique can produce several micrograms of target DNA from just a few nanograms of template DNA. Generally, five reagents are needed in a PCR reaction (Table 3.1).

1. Template DNA – contains the portion of DNA that we want to amplify.
2. DNA polymerase – a biological catalyst involved in the attachment of nucleotides to synthesize DNA. Responsible for driving the DNA synthesis.
3. Buffer – provides an optimal and stable chemical environment for the polymerase to work adequately.
4. Nucleotides (dNTPs) – the building blocks (A, T, C, and G) are added one by one to the new DNA strand by the DNA polymerase.
5. Forward and reverse primers – single-stranded DNA (ssDNA) that act as starting points for DNA elongation and synthesis. They anneal to the regions upstream (5') and downstream (3') of the DNA segment to be amplified.

Table 3.1. The components used for the PCR reaction using Phusion High-fidelity DNA polymerase and their final concentration in the PCR mixture.

Component	50 uL Reaction	Final Concentration
5X Phusion HF	10 uL	1 X
10 mM dNTPs	1 uL	200 uM
10 uM forward primer	2.5 uL	0.5 uM
10 uM reverse primer	2.5 uL	0.5 uM
Template DNA	Variable	< 250 ng
Phusion DNA polymerase	0.5 uL	1.0 unit/50 uL PCR
MilliQ water	To 50 uL	

Table 3.2. The components used for the PCR reaction using DreamTaq DNA polymerase. The DreamTaq Master Mix (2x) contains DreamTaq DNA polymerase, DreamTaq buffer, $MgCl_2$, and dNTPs.

Component	15 uL Reaction
DreamTaq Master Mix (2x)	7.5 uL
Forward primer	1 uL
Reverse primer	1 uL
Template	Variable
MilliQ water	To 15 uL

When the reagents (Table 3.1., Table 3.2) are mixed in the appropriate buffer, a cyclic protocol of heating (denaturing) and cooling (annealing) steps allow the DNA polymerase to copy the DNA in between the primers. PCR reactions start off with denaturation (Table 3.3, steps 1 and 2), where double-stranded DNA (dsDNA) is heated to the point by which H-bonds are broken between nucleotide base pairs resulting in ssDNA. The mixture is then cooled for the primers to anneal to the DNA template (Table 3.3, step 3). At this stage, the DNA polymerase initiates the synthesis of new DNA strands starting from the primers. The elongation temperature is increased to enable the DNA polymerase to synthesize and elongate the new target DNA strand accurately and rapidly (Table 3.3, step 4). Depending on the polymerase used, and whether it has proofreading capabilities or not, in addition to the length

of the gene, the time is adjusted per so. Phusion polymerase has a higher processivity compared to Taq polymerase, and displays a DNA synthesis rate of ~2 kb/min, whereas Taq polymerase synthesizes ~1 kb/min. After one cycle, each dsDNA molecule is composed of one new and one old DNA strand. The steps are then repeated 30 times (Table 3.3, step 5). The newly synthesized DNA segments serve as templates in subsequent cycles, allowing the DNA target to be exponentially amplified by millions. A final extension at 72°C is done to fill in any protruding ends of the newly synthesized strands (Table 3.3, step 6).

Table 3.3. Cycling conditions for the PCR reaction using Phusion High-fidelity DNA polymerase. Conditions when using DreamTaq DNA polymerase are shown in parentheses. The annealing temperature varies, depending on the primers melting point (Tm).

Step	Description	Temperature	Duration
1	Initial denaturation	98(95) °C	30(120) sec
2	Denaturation	98(95) °C	10(30) sec
3	Annealing	Primer Tm	15(30) sec
4	Primer extension	72°C	30(60) sec/kb
5	Step 2-4 repeated for 30 cycles		
6	Final extension	72°C	5 min
7	Hold	10(12) °C	Infinite

Phusion polymerase is a high-fidelity DNA polymerase engineered to have a lower error rate compared to Taq polymerase. By having a proofreading function, the Phusion polymerase can identify, and correct errors made during DNA synthesis. Thus, in this study, PCR reactions for cloning were carried out using Phusion High-fidelity DNA polymerase. DreamTaq DNA polymerase was used for all other PCR reactions.

3.2.1.1 Gel electrophoresis – DNA analysis

Gel electrophoresis is commonly used following a PCR reaction to verify whether the PCR reaction was successful. Gel electrophoresis is a method for separating DNA molecules based on their size. Each phosphate group in the DNA backbone contains a negatively charged oxygen, thus, the longer the DNA fragment is, the more negative it will be. This is exploited

in gel electrophoresis as negatively charged DNA is pushed by an electrical field towards a positive electrode, through an agarose gel containing small pores. Shorter DNA fragments move faster through the gel compared to longer fragments, and by running tests alongside a DNA size marker their approximate length can be determined.

In this study, gel electrophoresis was performed to visually confirm the presence of the desired DNA fragments following PCR reactions. Agarose gels were made of 0.7% agarose solution and stained with SYBR Safe DNA gel stain (Thermo Fischer Scientifc). PCR products were supplemented with Loading Dye 6X (Thermo Fischer Scientific) and run alongside SmartLadder MW-1700-10 (Eurogentec).

3.2.2 Transformation

To transform foreign DNA into a host cell, cells must be competent, i.e., cells able to take up foreign DNA molecules. In this study, transformation reactions were performed by heat shock using chemically competent *E. coli* E.cloni and by electroporation using electrocompetent *V. cholerae* C6706. The competent cells used in this study were prepared by others.

Preparing electrocompetent cells:

On day 1, *V. cholerae* were streaked onto LB plates from frozen stocks. On day 2, a single freshly streaked colony was inoculated into 5 mL LB and grown overnight. On day 3 the overnight cultures were diluted 1:100 into 400 mL of fresh LB without selection and grown until mid-exponential phase (OD_{600} = 0.35-0.40). Upon reaching the correct OD, the cells were immediately chilled down on ice to stop further growth. Cells were then split into two volumes of 200 mL and made electrocompetent by washing and pelleting five times in decreasing volumes of 10% glycerol (200 mL, 200 mL, 100 mL, 50 mL, and 20 mL). After the final wash, the pelleted cells were resuspended in 1 mL 10% glycerol, aliquoted into 80 uL samples, and flash frozen in liquid nitrogen. The competent cells were stored at -80°C.

Preparing chemically competent cells:

Chemically competent cells were grown and harvested identically to the electrocompetent cells, described above. After incubation on ice (1 hour) cells were washed in twice in 100 mL 100 m $MgCl_2$, concentrated by centrifugation at 4 ºC, and stored at -80 ºC.

3.2.2.1 Heat shock – chemical transformation

Heat shock transformation involves briefly heating the cells and the DNA mixture to a high temperature followed by rapid cooling on ice, where the thermal shock causes the bacterial cells to take up foreign DNA. This is a relatively quick and inexpensive method; however, it is generally less efficient compared to electroporation. As *V. cholerae* displays a defense system against plasmids (38) it was decided to first transform vectors into *E. coli* E.cloni before subsequently transforming the vectors into *V. cholerae.* The chemically competent *E. coli* E.cloni cells used in this study display high transformation efficiency. Therefore, when transforming *E. coli* E.cloni, heat shock was selected over electroporation mainly due to expenses, as a successful transformation was expected regardless of the transformation method.

Ligated products were added to chemically competent *E. coli* E.cloni, mixed carefully, and incubated on ice for 10 minutes. The cells were subjected to a heat shock at 42°C for 90 seconds, followed by 2 minutes on ice. Cells were then incubated in 500 uL LB (without selection/antibiotics) with shaking (225 rpm) for 1 hour. Transformants were plated on LB agar plates containing 25 mg/L chloramphenicol and incubated overnight. Subsequently, vector DNA was isolated using the QIAprep Spin Miniprep Kit (Qiagen) and the concentration of the isolated vectors was assessed using the NanoDrop™ (Thermo Fisher Scientific). Lastly, they were transformed into *V. cholerae* C6706 by electroporation.

3.2.2.2 Electroporation

Electroporation is a procedure by which foreign DNA is introduced into a host cell by passing through temporary pores in the cell membrane, created by an electrical pulse (Gene Pulser Xcell™, from Bio-Rad). Electroporation was selected over heat shock whenever transforming vectors into *V. cholerae* as this species has shown to dislike housing plasmids (38) and therefore are harder to transform. In short, approximately 10-20 ng of the isolated vectors were added to electrocompetent *V. cholerae* C6706, mixed carefully, and incubated on ice for 30 minutes. The cells were transferred to electroporation cuvettes (VWR International), and subjected to the electrical pulse, followed by incubation in 1 mL LB (without antibiotics) with shaking (225 rpm) for 1 hour. Transformants were selected on LB plates containing 5 ug/mL chloramphenicol and verified by Sanger sequencing (Genewiz) using primers P7 and P8 (Appendix A, Table A2).

3.3 Strain construction

In clinical isolates, genes encoding for β-lactamases are often present on large plasmids with low-copy numbers or encoded on the chromosome (39). To study the presence and effect of these enzymes on biofilm formation, a relatively low copy number (pA15 origin with ~15 copies/cell) was used, aiming to recreate the natural genetic environment of these genes. An overview of all strains used and constructed in this study can be found in Appendix A, Table A1.

3.3.1 Construction of the vector control (pCTRL)

The vector used in this study is a low-copy number vector (called from here on pUN) with a chloramphenicol resistance marker (pA15 origin with ~15 copies/cell) and has been described previously (40). Briefly, whole vector amplification was performed, and the PCR product was digested with LguI and DpnI by recirculation using T4 ligase. The ligated product was transformed into *E. coli* E.cloni® 10G (MP21-05). Transformants were selected on LB plates containing 25 mg/L chloramphenicol and verified by Sanger sequencing. Subsequently, the vector was transformed into *V. cholerae* C6706 by electroporation (named pCTRL).

LguI is a restriction enzyme that recognizes the sequence CTAG and cuts between the C and T nucleotides on both strands, resulting in sticky ends. DpnI is a restriction endonuclease enzyme that recognizes and cleaves DNA containing the Gm6ATC sequence and is commonly used in molecular biology to digest methylated DNA. Gm6ATC is a specific sequence of DNA nucleotides, which refers to guanine (G) followed by methylated adenine (m6A), thymine (T), and cytosine (C). Mutated DNA from the PCR reaction will not be affected by DpnI as only non-mutated template is methylated.

To obtain alternative vector controls, two additional vectors were constructed (named pCTRL2 and pCTRL3), both harboring larger vectors than the initial pCTRL. Both pCTRL2 and pCTRL3 contain an identical vector backbone compared to pCTRL. In addition, pCTRL2 carries the promoter without a *bla* gene and pCTRL3 harbors the $bla_{\text{KPC-2}}$ gene with an inactive promotor.

For the construction of pCTRL2, whole-vector amplification was performed, using the pUNe4-vector and primers P3 and P4 (Appendix A, Table A2). PCR was conducted with

Phusion polymerase (NEB), and PCR settings were optimized according to the length of the gene. To ensure the PCR was successful, gel electrophoresis was conducted, followed by DNA purification using QIAquick® Spin Columns Kit. The concentration was measured using NanoDrop^{TM} to calculate the correct amount to use for the ligation. The blunt-ended vector DNA was ligated using T4 Ligase (Thermo Fischer Scientific), without prior digestion, and transformed into chemically competent *E. coli* E.cloni by heat shock. The rest was performed as for pCTRL in 3.3.1.

For the construction of pCTRL3, the *bla*$_{KPC-2}$ vector was amplified using primers P112 and P113 (Appendix A, Table A2). The rest was performed as for pCTRL in 3.3.1.

3.3.2 Construction of the β-lactamases

The genes encoding for the eight β-lactamases used in this study were either synthesized (*bla*$_{TEM-1}$, *bla*$_{CTX-M-15}$, *bla*$_{NDM-1}$, and *bla*$_{CMY-2}$, Genewiz. NG_050145.1, NG_048935.1, NG_049326.1, and NG_048814.1 respectively (23)) or originated from clinical isolates (*bla*$_{KPC-2}$, *bla*$_{VIM-2}$, *bla*$_{OXA-48}$, and *bla*$_{OXA-163}$) (41-44). pUN-*bla*$_{TEM-1}$ was constructed in this study (by Rebekka Rolfsnes, unpublished study), whereas the remaining constructs have been published previously (23). Generally, the recombinant vectors were constructed by expressing the *bla*-genes in *E. coli*, using the pUN vector described in 3.3.1. This was done by removing a restriction site (NcoI) from the original vector's chloramphenicol resistance marker using site-directed mutagenesis. To subclone β-lactamase genes, primers were designed to insert a new NcoI site at the start codon of each *bla*-gene. The vector backbone and gene inserts were amplified, followed by NcoI/XhoI/DpnI digestion, and finally ligated together using T4 ligase for 1 hour at room temperature. Finally, the ligated product was transformed into E. *coli* and confirmed by Sanger sequencing. In this study, the vector constructs, harboring the *bla*-gene of interest, were transformed into electrocompetent *V. cholerae* C6706 and transformants were selected on LB plates containing 5 mg/L chloramphenicol. PCR amplification and gel electrophoresis analysis were performed to ensure a successful transformation and constructs were confirmed by Sanger sequencing.

3.3.3 Construction of the mutational KPC-2 library

The KPC mutant library used in this study was constructed using error-prone PCR to introduce mutations in the *bla*$_{KPC-2}$ gene and has been published (23). In short, vector DNA was used and mutagenic nucleotides (oxo-dGTP for transversions and dPTP for transitions) were added to the PCR reaction mix with specific primers. The PCR products were DpnI-digested, and 5 ng of each product was used for a second PCR, which was performed without mutagenic nucleotides. The second PCR product was then digested with NcoI and XhoI and ligated in a 1:3 ratio with the digested and purified vector backbone. The resulting ligation mixture was transformed into *E. coli* E. cloni. To ensure that the entire sequence space, theoretically, could be sampled, ≥5000 mutants were harvested and included in the mutant library. In this study, 10 ng of the mutant library was transformed into *V. cholerae* C6706 by electroporation, and transformants were selected on LB plates containing 5 mg/L chloramphenicol. Library sizes were determined by cell counts and ≥5000 colonies were harvested.

3.3.4 Sub-cloning of mutants C2$_{selected}$ and C3$_{selected}$

The re-cloning of C2$_{selected}$ and C3$_{selected}$ was done to isolate the effect of their genes from potential confounding effects such as chromosomal mutations or changes in the vector backbone. After selection of the mutants, vector DNA was isolated following the manual of the QIAprep® Spin Miniprep. The *bla*$_{KPC}$ genes were amplified using primers P7 and P8 (Appendix A, Table A2), and Phusion polymerase, followed by PCR purification using QIAquick® Spin Columns. 500 ng of the template DNA was digested with DpnI, XhoI, and NcoI (Thermo Fischer Scientific), followed by DNA purification as mentioned above. The concentration of the extracted DNA was assessed using the NanoDrop^{TM}. 24 ng of the digestion product was then ligated with 20 ng of the backbone, which was amplified using primer 3 and 4 (Appendix A, Table A2) but otherwise prepared similarly to the insert, using T4 Ligase. Transformation into the *E. coli* E. cloni and the subsequent transfer into *V. cholerae* was performed as for pCTRL in 3.3.1.

3.3.5 Construction of KPC-2:S70A and $C2_{re\text{-}cloned}$:S70A

Active-site serine of KPC-2 was mutated to alanine (S70A) using whole vector site-directed mutagenesis with primers, P115 and P108, containing LguI cutting sites (Appendix A, Table A2) to investigate whether disruption of the enzymatic activity would affect biofilm formation. The $bla_{KPC\text{-}2}$ genes were amplified using primers P115 and P108 (Appendix A, Table A2) and Phusion polymerase. The PCR products were digested with LguI (Thermo Fischer Scientific) and DpnI for 1 hour at 37°C following self-ligation using T4 ligase. Transformation into *V. cholerae* C6706 was performed as for pCTRL in 3.3.1.

3.4 Antibiotic susceptibility tests

To assess the functionality of the constructed β-lactamases in the target strain, antimicrobial susceptibility was determined. The Minimum Inhibitory Concentration (MIC), which represents the minimum antibiotic concentration needed to inhibit 100% visual bacterial growth, of ampicillin against the strains was determined using MIC Test Strips (Liofilchem). In short, a bacterial suspension with an optical density of 0.5 McFarland was prepared. Using a cotton swab, the solution was spread on LB agar plates for confluent growth followed by an antibiotic gradient strip placed on the agar plate for MIC determination. MIC values were determined by visual inspection as the concentration at which no bacterial growth was observed. When determining ampicillin MICs, LB agar plates *with* 5 mg/L chloramphenicol were used to ensure vector maintenance.

When performing this assay, it is recommended to use Müller Hinton agar plates for determining MICs. However, as this study aimed to investigate the differences between the strains, rather than clinically relevant MICs, LB agar plates were used.

3.5 Biofilm quantification by crystal violet staining

Biofilm formation was investigated and quantified by crystal violet dye staining where the optical density of stained biofilm was determined spectrophotometrically.

Initially, bacteria were streaked from frozen stocks onto LB agar plates and incubated overnight at 37°C. On day 2, sterile toothpicks were used to inoculate a single colony into a 96-deep well plate with 1 mL LB in each well. Cultures were grown overnight at 37°C with shaking (700 rpm). On day 3, overnight cultures were diluted 1:100 (20:1980 uL) into a 24-well plate (Thermo Fischer Scientific) containing fresh media. Plates were incubated statically for 24 hours at 37°C. On day 4, the culture medium was removed by inverting the plate into the trash followed by the removal of non-adherent cells by submerging the plate in a wash tray containing dH_2O three times. Biofilms were then fixed by incubating the plate for 1 hour at 55°C. Biomass was stained with 2.1 mL 0.1% CV and left at room temperature for 10 minutes. After the removal of excess CV by emptying in the trash, the plate was submerged again in a wash tray as mentioned above to remove excess CV. The stained biomass was solubilized by adding 2.25 mL of 70% EtOH to each well. After 30 minutes the OD was measured at 595 nm using an Epoch or Spark plate reader (Epoch 2, BioTek and Spark, Tecan). To minimize background interference the mean OD value of the negative controls (EtOH) was subtracted from the values of the test wells during analysis.

The first two times this assay was performed, the assay was performed as described above, however, the OD_{595} was *measured* in 96 microtiter plates (200 uL was transferred from the 24-well plate to the 96 microtiter plate). All the following results were measured directly in the 24-well plates. Due to this, the values from the 24-well plates have been multiplied with a factor of 0.6 due to the ratio differences of the wells. Thus, Figure 4.1B and Appendix B represent values multiplied by 0.6. All remaining values presented are 24-well values.

3.6 Bacterial growth curve assay

To investigate the growth rate and carrying capacity of each strain, growth curve assays were performed. Strains were streaked for isolation and incubated overnight at 37°C. Single colonies were inoculated into 1 mL LB in a 96-deep well plate and incubated overnight at 37°C with shaking (700 rpm). Three biological replicates per strain were included. The following day, overnight cultures were diluted 1:100 (10:990 uL) into fresh LB in a new 96-

deep well plate. Then, three technical replicates per biological replicate were inoculated into a 100-well Honeycomb plate (Oy Growth Curves Ab Ltd.). The plate was incubated at 37°C with continuous shaking for 24 hours. Growth was monitored by OD_{600} measures every fourth minute in a Bioscreen machine (Oy Growth Curves Ab Ltd.). The exponential growth rates were calculated by measuring the optical densities of bacterial cultures as a function of time.

3.7 Biofilm pellicle assay

Overnight cultures of the strains were prepared from frozen glycerol stocks in a 15 mL culture tube containing 3 mL LB medium and incubated overnight at 37 °C with shaking (700 rpm). The following day, overnight cultures were diluted 1:100 (20:1980 uL) in fresh LB medium in a 24-well plate and incubated statically at 37°C for 24-48 hours. Pellicle formation was identified visually and documented graphically after 24 and 48 hours.

3.8 Biofilm pellicle evolution

Overnight cultures of strains were prepared from frozen glycerol stocks in either a 15 mL culture tube containing 3 mL LB medium or into a 96-deep well plate with 1 mL LB in each well and incubated overnight at 37°C with shaking (700 rpm). The next day, overnight cultures were diluted 1:100 (20:1980 uL) in fresh LB medium in a 24-well plate and incubated statically at 37°C for 48 hours. Pellicle formation was identified visually and documented graphically after 48 hours.

Using an inoculation loop, pellicles were harvested from the top of the culture, avoiding the culture medium, and resuspended in 1 mL PBS. The PBS solution containing the biofilm pellicles was then vortexed for 2 minutes to disrupt the biofilm pellicles and dislodge biofilm-embedded cells. An inoculation loop was used to streak out liquid from the bacterial PBS solution onto an LB agar plate for the isolation of pellicle-evolved clones. To harvest the remaining biofilm-evolved population, overnight cultures of the pellicle-PBS-solution were then made by adding 990 uL of the solution and 4000 uL LB media and incubated for 18h ± 2h at 37 °C with shaking (700 rpm).

3.9 Statistical analysis

The normality of the datasets was investigated by the Shapiro-Wilk test and by visual inspection of the residual plots. Datasets were analyzed using a one-way ANOVA and Dunnett's multiple comparisons tests. Statistical significance was determined by $\alpha=0.05$. To compare any two means an unpaired t-test (two-tailed P value) was used. Both comparison tests assume normality (normally distributed data). All biofilm formation assays were performed using at least four independent biological replicates. Growth curve assays were performed with three biological replicates per strain, with three technical replicates per biological replicate. All statistical analyses were performed using GraphPad Prism Version 9.

4 Results

Biofilm formation is key to the success of the enteric pathogen *V. cholerae* which has caused several large cholera outbreaks in recent decades and has the ability to express β-lactamase genes (26, 45). While the production of β-lactamases has been shown to inhibit biofilm formation in clinically important pathogens such as *Escherichia coli* and *Pseudomonas aeruginosa*, little is known about the generality of this observation (8). Therefore, I aimed to assess how the production of these enzymes affects biofilm formation in *V. cholerae*. To assess biofilm formation in *V. cholerae*, eight β-lactamases, spanning all Ambler classes: KPC-2, TEM-1, CTX-M-15 (class A), NDM-1, VIM-2 (class B), CMY-2 (class C), OXA-48, and OXA-163 (class D), were selected for investigation. The *bla* genes were subcloned into a low copy number vector (origin of replication: pA15, approximately 15 copies per cell) (40), and constructs were confirmed with Sanger sequencing. To control for vector-mediated effects on biofilm formation, a vector control was constructed, only containing the vector backbone and no *bla* genes.

4.1 β-lactamases are functional in *Vibrio cholerae*

The functionality of all these enzymes in the target strain was assessed by determining the antimicrobial susceptibility (MICs) towards the β-lactam ampicillin using MIC test strips (Table 4.1). Constructed strains carrying *bla* genes were compared to the ancestral *V. cholerae* (wtVC) strain and the strain carrying the vector control (pCTRL). As expected, wtVC and the pCTRL displayed similar ampicillin resistance profiles with a MIC of 3-4 mg/L. In comparison, all *bla*-carrying strains displayed substantially decreased ampicillin susceptibility (6- to 64-fold) and were all resistant according to the EUCAST breakpoint (>8mg/L) (46). In detail, the production of KPC-2, CTX-M-15, NDM-1, VIM-2, OXA-48, and OXA-163 resulted in the largest changes in susceptibility (64-fold). On the contrary, the expression of $bla_{\text{TEM-1}}$ and $bla_{\text{CMY-2}}$ affected resistance development to a lesser degree (6-fold and 8-fold, respectively). Thus, the constructed strains showed appropriate susceptibility antibiotic profiles, demonstrating proper expression and functionality of all β-lactamases in *V. cholerae.*

Table 4.1. Ampicillin MIC determination. *bla* genes were expressed in *V. cholerae* (wtVC) and MIC values are reported as mg/L.

Strain/β-lactamase	Ampicillin MIC (mg/L)
wtVC	4
pCTRL	3-4
KPC-2	>256
TEM-1	24
CTX-M-15	>256
NDM-1	>256
VIM-2	>256
CMY-2	32
OXA-48	>256
OXA-163	>256

4.2 Expression of β-lactamases reduces biofilm formation in *Vibrio cholerae*

4.2.1 β-lactamases suppress surface attachment and biofilm pellicle formation in *V. cholerae*

To test if the expression of these enzymes affects biofilm formation in *V. cholerae*, a crystal violet assay was used to quantify biofilm formation in all the β-lactamase-producing strains. In addition, their ability to form biofilm pellicles in static liquid cultures was also assessed. To isolate the effect of the β-lactamases (on biofilm formation), the *bla*-producing strains were compared to pCTRL. For comparative purposes, wtVC was also included. Prior to testing for statistical significance, datasets were tested for normal distribution using a Shapiro-Wilk. The datasets for each strain had a log-normal distribution rather than a normal distribution. After log transformation, all strains passed the Shapiro-Wilk test of log normality, thus meeting ANOVA's assumption of normality. To test for statistical significance, a one-way ANOVA and Dunnett's multiple comparisons tests were conducted ($\alpha = 0.05$).

Firstly, the introduction of the low copy number vector into wtVC (pCTRL) resulted in a significant reduction in biofilm formation ($P<0.0001$) (Figure 4.1B and Appendix B). Compared to pCTRL, almost all *bla*-producing strains displayed a significant decrease in biofilm formation (Figure 4.1B and Appendix B). In detail, all β-lactamases from class A; KPC-2, TEM-1, and CTX-M-15, as well as VIM-2 (class B), CMY-2 (class C), and both β-lactamases from class D; OXA-48, and OXA-163 produced significantly less biofilm relative to pCTRL after 24 hours of static incubation ($P<0.0001$). Expression of $bla_{\text{NDM-1}}$ did not affect biofilm formation significantly ($P=0.9940$)

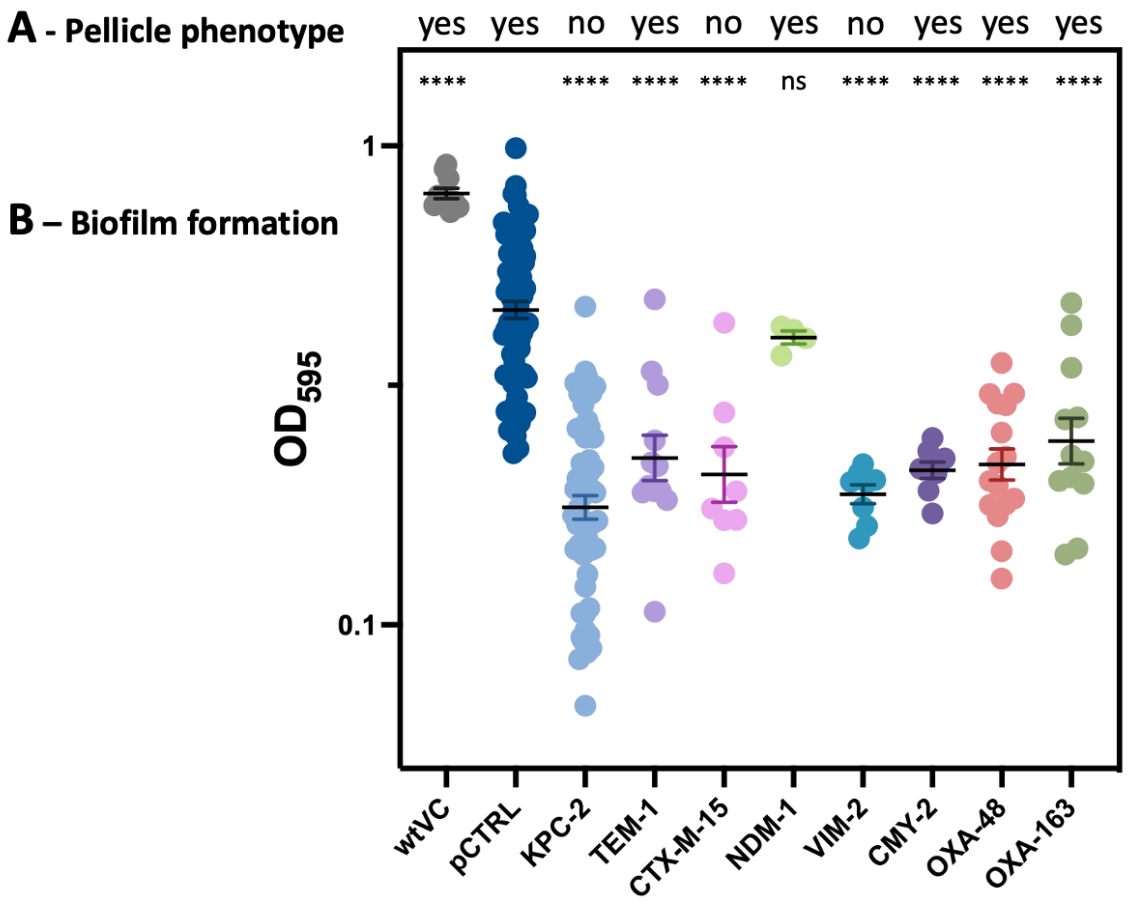

Figure 4.1. **(A)** The strains' pellicle phenotype after 24 hours of static incubation is scored as yes or no. For graphical documentation of pellicles, see Figure 4.2. **(B)** Static biofilm formation of wtVC and *bla*-expressing strains compared to pCTRL. The strains are presented on the x-axis and OD_{595nm} values are presented on the log y-axis. Each dot represents the OD of a single biological replicate. Bars represent the average, and error bars represent the standard error of the mean (SEM). Sample size as followed: wtVC, n=10; pCTRL, n=77; KPC-2, n=56; TEM-1, n=12; CTX-M-15, n=8; NDM-1, n=4; VIM-2, n=8; CMY-2, n=8; OXA-48, n=16; OXA-163, n=12. Data were analyzed using one-way ANOVA and Dunnett's multiple comparisons tests. Statistical significance is indicated by asterisks as follows: **** P<0.0001. ns = not significant.

The strain's biofilm formation capacity was also assessed by the ability of the strains to form biofilm pellicles. The resulting pellicles after 24 and 48 hours were identified visually and are presented in Figure 4.2. Generally, results obtained from CV staining and pellicle formation agreed well with each other (Figure 4.1B and Figure 4.2). After 24 hours of static incubation, wtVC produced a strong and stable pellicle at the air-liquid interface (Figure 4.2). While the pCTRL strain was still able to produce a visible pellicle, the pellicle was substantially weaker

and thinner than wtVC. Similarly, the production of all β-lactamases, except for NDM-1, reduced pellicle formation substantially compared to the wtVC strain. KPC-2, CTX-M-15 and VIM-2 did not form a pellicle after 24 hours. The remaining strains did form pellicles after 24 hours, to various extents; pCTRL, TEM-1, CMY-2, OXA-48, and OXA-163 produced pellicles that seemed to grow from the edges of the well towards the middle, without covering the entire air-liquid interface. wtVC and NDM-1 however, formed pellicles extending across the entire air-liquid interface. After 48 hours, all strains formed pellicles that extended across the entire air-liquid interface. Biofilm pellicles formed by wtVC, TEM-1, CMY-2, OXA-48, and OXA-163 displayed greater structural integrity compared to the remaining strains. Taken together, β-lactamases from all Ambler classes suppress both surface attachment (CV-staining) and biofilm pellicle formation in *V. cholerae*.

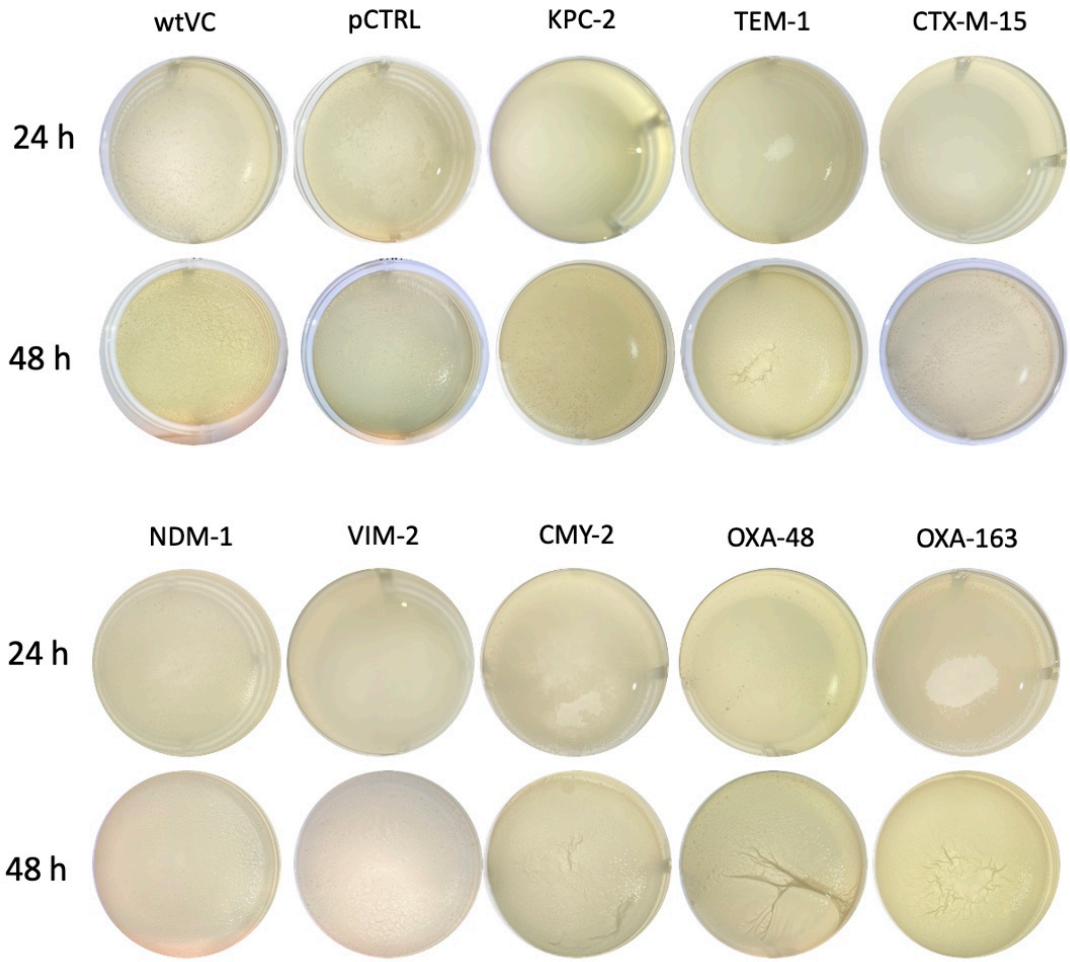

Figure 4.2. Morphology of biofilm pellicles of wtVC, pCTRL, KPC-2, TEM-1, CTX-M-15, NDM-1, VIM-2, CMY-2, OXA-48, and OXA-163 after 24 and 48 hours of static incubation at 37°C.

4.2.2 Poor correlation between biofilm formation and fitness cost

To rule out the possibility of growth defects causing the observed decrease in biofilm formation, the growth rate was measured using growth curve assays. To quantify the fitness cost, the strains' exponential growth, lag phase, and carrying capacity were measured (Table 4.2 and Figure 4.3). wtVC was used as the reference.

First, I investigated how the exponential phase growth was affected in the vector control and the β-lactamase-producing strains. Introduction of the vector control into wtVC led to a reduction of 16% in growth rate, a substantial impact on exponential growth (Table 4.2). In fact, pCTRL exhibited the lowest exponential growth out of all tested samples. The

expression of β-lactamase genes was either neutral to the exponential growth (NDM-1, CMY-2, OXA-48, and OXA-163) or even restored the vector-induced growth deficiency (KPC-2, TEM-1, CTX-M-15, and VIM-2). Similarly, the carrying capacity of pCTRL was found to be lower than wtVC (Table 4.2). Also here, the presence of β-lactamases was often either neutral or partially restored the reduction. Only the production of TEM-1 and NDM-1 led to carrying capacities substantially lower than pCTRL (Table 4.2 and Figure 4.3C, and 4.3E respectively). Lastly, the presence of pCTRL doubled the growth lag time compared to wtVC (Table 4.2 and Figure 4.3A). Also here, the expression of many β-lactamase genes compensated for the increase in lag time. Only the presence of TEM-1 and CMY-2 resulted in lag times substantially longer than wtVC (Figure 4.3C and 4.3G respectively).

Table 4.2. Results from growth curve assays. The growth rate value is relative to the reference *V. cholerae* strain (wtVC = 1). Carrying capacity is the maximum OD reached during 24 hours. The average time in the lag phase is presented in minutes. Shown results are averaged values of 6 biological replicates where each biological replicate was determined in three technical replicates.

Strain/β-lactamase	Relative growth rate	Carrying capacity (maximum OD_{600})	Time in lag phase (min)
wtVC	1	1.393	120
pCTRL	0.839	1.111	256
KPC-2	0.966	1.200	128
TEM-1	1.072	0.935	182
CTX-M-15	0.987	1.148	126
NDM-1	0.863	0.830	126
VIM-2	1.021	1.158	112
CMY-2	0.852	1.076	415
OXA-48	0.876	1.222	114
OXA-163	0.881	1.043	130

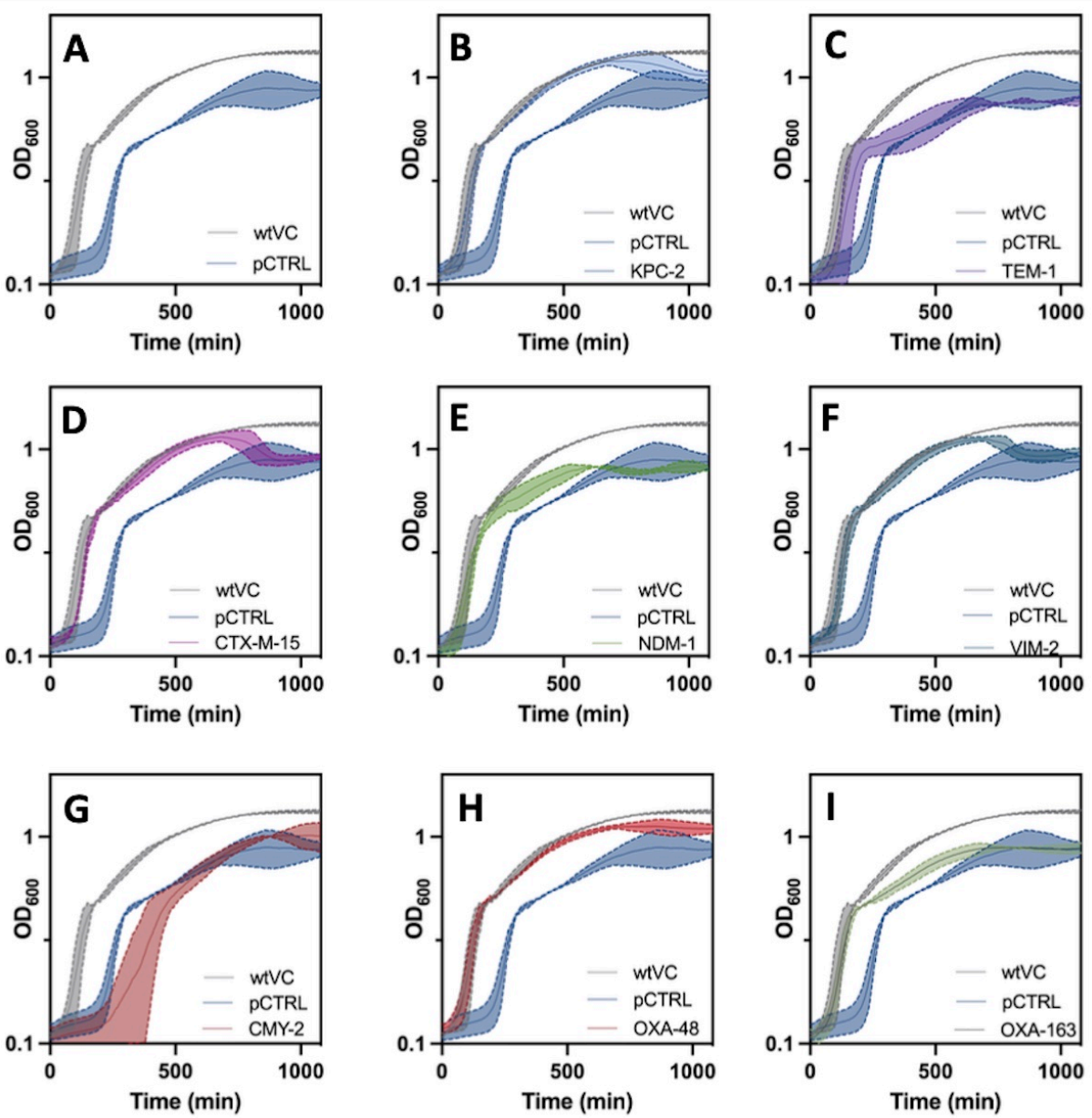

Figure 4.3. Growth curves. wtVC (grey) and pCTRL (dark blue) are shown in each graph for comparison. **(A)** wtVC (grey) *versus* pCTRL (dark blue). **(B)** wtVC *versus* KPC-2 (light blue). **(C)** wtVC *versus* TEM-1 (purple). **(D)** wtVC *versus* CTX-M-15 (pink). **(E)** wtVC *versus* NDM-1 (dark green). **(F)** wtVC *versus* VIM-2 (turquoise). **(G)** wtVC *versus* CMY-2 (light red). **(H)** wtVC *versus* OXA-48 (dark red). **(I)** wtVC *versus* OXA-163 (light green). Time (min) and OD_{600} values are presented on the x- and log y-axis, respectively. Error bars represent the standard deviation (SD) of the mean of six biological replicates. Data were analyzed, and figures were created, using GraphPad Prism version 9.

Based on these results, the aim was to understand whether changes in growth properties could explain the changes in biofilm formation described in Chapter 4.2.1. For that, the (linear) correlation between the $\log_{10}$ distributed OD_{595} values from the CV-assay (Figure 4.1B and

Appendix B) and either the relative growth rate, carrying capacity, or lag phase was investigated (Figure 4.4A, 4.4B, and 4.4C respectively). The regression coefficients (R) ranged between <0.01 and 0.15 (Figure 4.4) indicating the observed changes in growth are not responsible for the observed changes in biofilm formation.

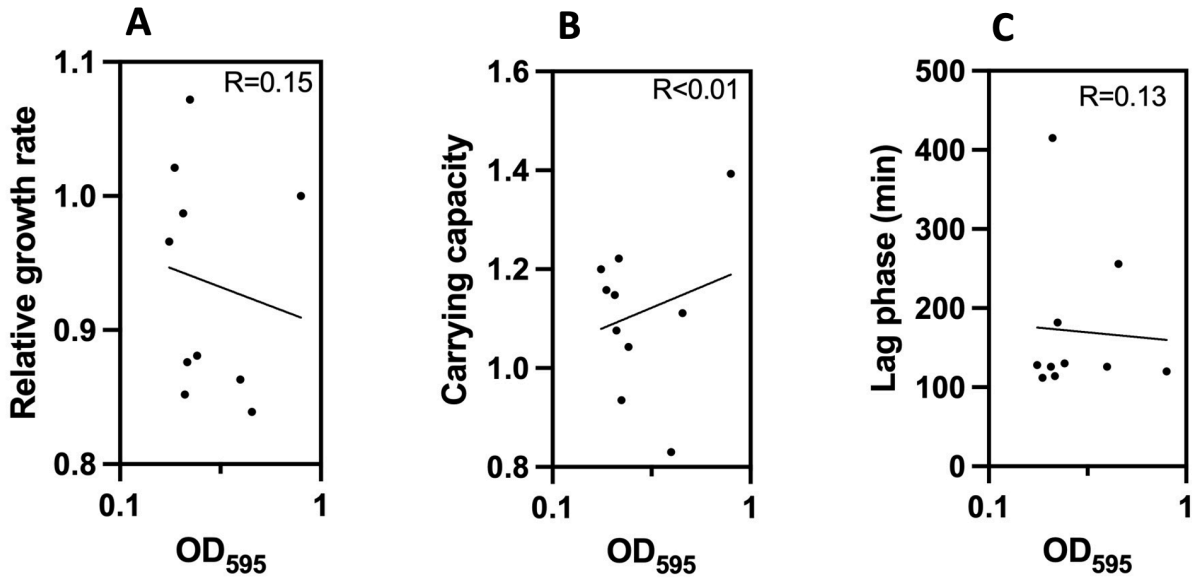

Figure 4.4. Showing the linear correlation, denoted by the correlation coefficient (R), between $\log_{10}$ OD_{595} values from the CV assay (Figure 4.1B and Appendix B) and A: relative growth rate, B: carrying capacity, and C: lag phase. **(A)** the relative growth rate is presented as OD_{600} values on the y-axis. The correlation coefficient indicates a poor correlation (R=0.15). **(B)** Carrying capacity is presented as OD_{600} values on the y-axis. The linear correlation was considered negligible (R<0.01). **(C)** The lag phase is presented as minutes on the y-axis. The correlation coefficient indicates a poor correlation (R=0.13). Data were analyzed, and figures were created, using GraphPad Prism version 9.

4.2.3 Chloramphenicol resistance remains stable across different *bla* encoding vectors

The pUN vector carried a chloramphenicol resistance gene marker on the backbone. To ensure the stability of the *bla*-encoding vectors in *V. cholerae*, all vector-carrying strains were consistently grown in medium supplemented with chloramphenicol (5 mg/L). I hypothesized that fluctuations in chloramphenicol resistance could result in the observed changes in lag phases and fitness (Table 4.2 and Figure 4.3). To exclude that, antibiotic susceptibility tests

towards chloramphenicol were performed. The MIC strip test was performed using LB agar plates without chloramphenicol, to avoid an additive effect of chloramphenicol.

As expected, the wtVC strain displayed low chloramphenicol resistance (1 mg/L). In comparison, all vector-carrying strains exhibited chloramphenicol susceptibility of 192 to >256 mg/L. Interestingly, two of the tested strains, pCTRL and CMY-2, showed two inhibition zones on the MIC agar plate (Table 4.3, Figure 4.5A and 4.5B). The second inhibition zone roughly matched the susceptibility of wtVC. This could indicate that these two vectors are lost in parts of the population due to the higher instability of the vectors. There seemed to be a correlation between the number of inhibition zones and the extended lag phases seen for pCTRL and CMY-2. The remaining strains displayed MICs >256 mg/L (Table 4.3 and Figure 4.5C). However, the chloramphenicol concentration used in all assays was far below the MIC of the vector-carrying strains and 5-fold higher than the wtVC. Thus, the chloramphenicol concentration should not have a large confounding effect on the observed changes in biofilm formation.

Table 4.3. Chloramphenicol MIC determination and the number of inhibition zones. β-lactamase genes are expressed in *V. cholerae* C6706 and MIC values are reported in mg/L. Parentheses indicate the MIC value of the second inhibition zone. For graphical documentation of inhibition zones see Figure 4.5.

Strain/β-lactamase	Chloramphenicol MIC (mg/L)	No. of inhibition zone(s)
wtVC	1	1
pCTRL	192-256 (1.5)	2
KPC-2	>256	1
TEM-1	>256	1
CTX-M-15	>256	1
NDM-1	>256	1
VIM-2	>256	1
CMY-2	>256 (3)	2
OXA-48	>256	1
OXA-163	>256	1

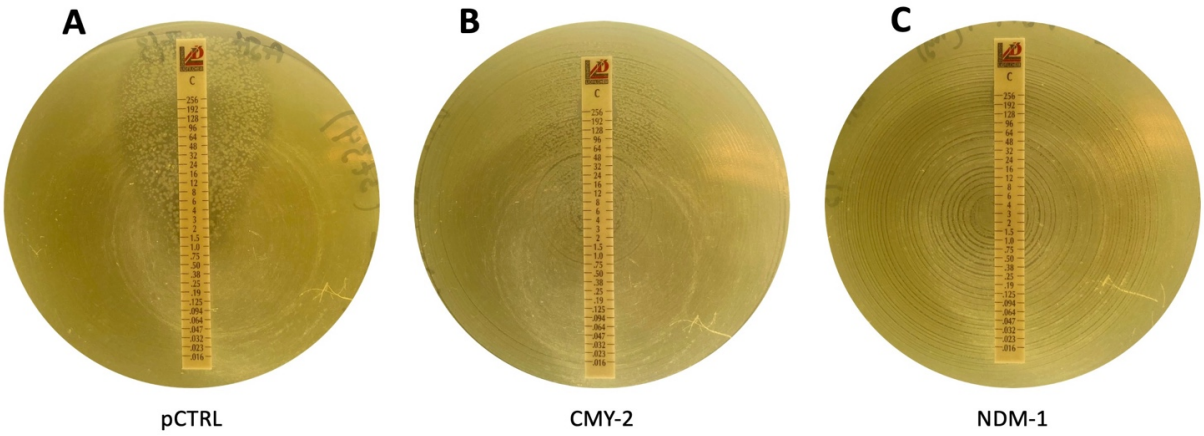

Figure 4.5. Chloramphenicol MIC determination using MIC strip test. **(A)** pCTRL showing two inhibition zones. **(B)** CMY-2 shows two inhibition zones, although not as visible as pCTRL. **(C)** NDM-1 is included for comparison. All the remaining β-lactamases displayed similar MICs as NDM-1 with MICs > 256 mg/L.

4.2.4 Increased size of vector control negatively impacts the lag phase in *V. cholerae*

The pCTRL control used in this study represents a circular vector with the pA15 origin and the chloramphenicol resistance gene. Both β-lactamase genes and the promotor to express these genes were removed. The results from 4.2.1 to 4.2.3 indicate that the introduction of the vector into wtVC has a relevant effect on both biofilm development and growth. Recently, it has been described that *V. cholerae* possesses an extensive plasmid defense system (38). To construct a more representative control vector (vectors with *bla* genes are larger than the original pCTRL), pCTRL2 and pCTRL3 were constructed. While pCTRL2 and pCTRL3 contained an identical vector backbone compared to pCTRL, pCTRL2 carried the promoter without a *bla* gene and pCTRL3 harbored the bla_{KPC-2} gene with inactive promoter.

Firstly, single colonies formed by both pCTRL2 and pCTRL3 were notably smaller than pCTRL-colonies. In addition, there was a qualitative difference between *V. cholerae* harboring pCTRL2 and pCTRL where cells with pCTRL3 grew even slower than cells with pCTRL2. Due to this observation, only pCTRL2 was subjected to a growth curve assay as

well as biofilm quantification by CV staining. This observation was supported by growth curve results, which revealed an even longer lag phase for pCTRL2 relative to pCTRL (4.6A). These results indicate that the insertion of the promoter and/or *bla* gene with a deactivated promoter did not positively affect growth and the growth defect of pCTRL remains elusive.

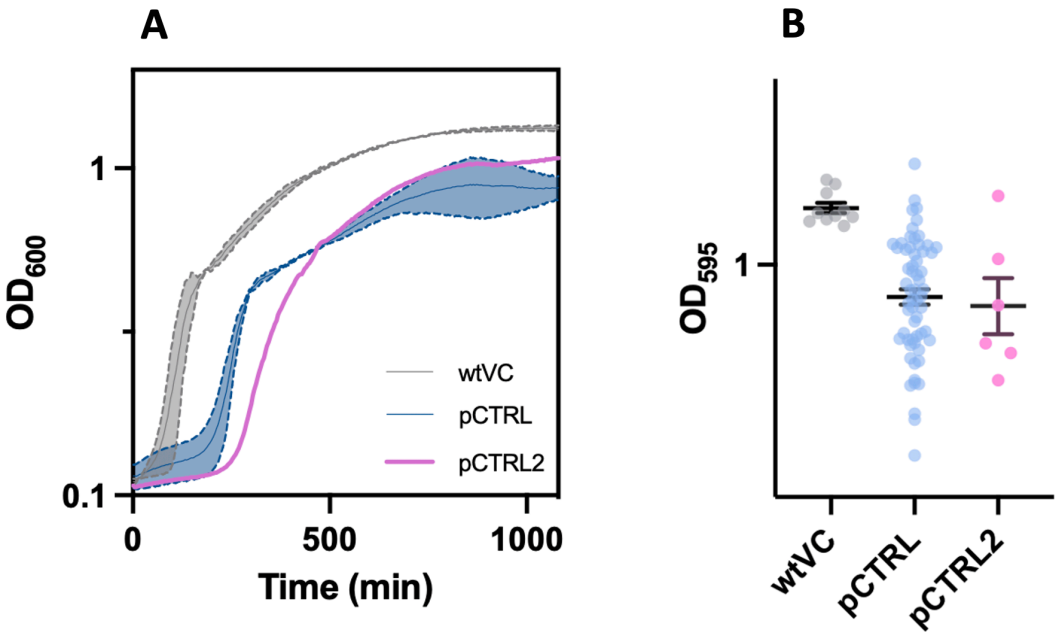

Figure 4.6. Growth curves and static biofilm formation of pCTRL, pCTRL2, and wtVC. **(A)** Growth curve showing pCTRL (dark blue) *versus* pCTRL2 (pink). wtVC (grey) is shown for comparison. Time (min) and OD_{600} values are presented on the x- and log y-axis, respectively. Error bars represent the standard deviation (SD) of the mean of 3-6 biological replicates (wtVC and pCTRL, n=6; pCTRL2, n=3). **(B)** Static biofilm formation of pCTRL, pCTRL2, and wtVC after 24 hours. The strains are presented on the x-axis and OD_{595nm} values are presented on the log y-axis. Each dot represents the OD of a single biological replicate. Bars represent the average, and error bars represent the standard error of the mean (SEM). Sample size as followed: wtVC, n=10; pCTRL, n=61; pCTRL2, n=6. The means of pCTRL and pCTRL2 were compared and found to be non-significant (unpaired t-test (P=0.7221). Data were analyzed, and figures were created, using GraphPad Prism version 9.

4.3 The evolution of KPC-2 and its influence on biofilm formation

The observed negative effects on biofilm formation in *V. cholerae* are in line with previous studies in other Gram-negative pathogens (8, 36). Next, I wanted to investigate if this effect was related to the function of the β-lactamases and if the evolution of β-lactamases can compensate for their observed negative effect on biofilm formation. KPC-2 was chosen as this β-lactamase had the strongest negative effect on biofilm formation (Figure 4.1B and Appendix B). In addition, this is a β-lactamase often encoded on plasmids that are circulating in clinically relevant pathogens (e.g., *Klebsiella pneumoniae*) that are adept biofilm formers *in vitro* and *in vivo* (41).

Direct evolution is a powerful method to fast-forward the natural evolution of proteins in a laboratory setting (21). This makes it an ideal method to test how the evolution of β-lactamases affects biofilm formation. In order to conduct directed evolution of KPC-2, error-prone PCR was used to construct a mutational library of KPC-2 that averaged 1-2 non-synonymous mutations per allele. The bla_{KPC-2} mutant library was previously constructed (23). In short, a PCR was performed in two rounds; the first PCR round used mutagenic nucleotides that lead to the accumulation of mutations within the target gene. During the second round of PCR, non-mutagenic nucleotides were used to replace the mutagenic ones and fix the final mutations. In this study, the mutational library was transformed into *V. cholerae* and ≥ 5000 colonies were harvested to ensure that the entire sequence space, in theory, could be sampled.

4.3.1 Screening of the KPC-2 mutational library

In total, biofilm formation in 129 KPC-2 mutants was screened in one biological replicate using crystal violet staining. The KPC-2:library mutants were compared to the distribution of KPC-2 (n=61) (Figure 4.7). The Shapiro-Wilk test was used to test for normality and lognormality. The data were log-transformed, and all strains passed the Shapiro-Wilk test of log normality. To test for statistical significance, an unpaired t-test (α=0.05) was used when comparing two log means. The means of the library and KPC-2 were found to be significantly different (unpaired t-test, P=0.0131. Figure 4.7A).

Based on these results, 19 mutants (presented as red dots in Figure 4.7A) at the outer tails of the distribution were randomly selected, and their biofilm-forming capacity was quantified in at least 4 biological replicates. However, verification of mutants was challenging due to the high degree of variation (illustrated in Figure 4.7B). The red dots in Figure 4.7B represent the initial screening OD value of the 19 outliers (obtained from three screening assays performed on different days), whereas the remaining black dots are OD values from subsequent verification assays. Only one significant finding was found after the first rounds of verification; mutant 19 (M19) displayed significantly increased biofilm formation relative to KPC-2 (one-way ANOVA, $P<0.0001$), whereas the remaining 18 mutants did not affect biofilm formation significantly.

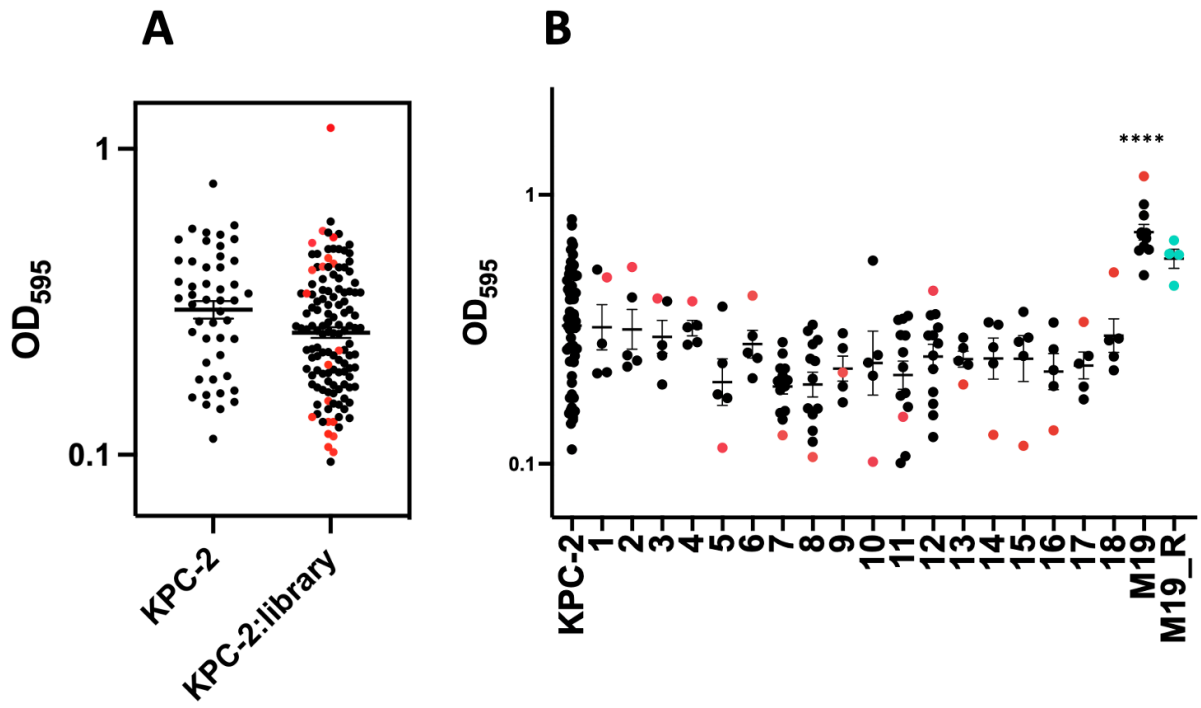

Figure 4.7. Biofilm development mediated by in KPC-2 versus KPC-2 mutants. Strains are presented on the x-axis and OD_{595nm} values from CV biofilm staining are presented on the log y-axis. Each dot represents the OD of a single biological replicate. The red dots represent the initial screening OD value for each mutant. Error bars represent the standard error of the mean (SEM). Sample size: KPC-2, n=61; KPC-2:library, n=129; Mutant 1 to 6, 9, 10, and 13 to18, n=5; Mutant 7, 8, 11, and 12, n=13; Mutant 19, n=11; $Mutant19_{retransformed}$, n=4. **(A)** The means of KPC-2 and KPC-2:library were analyzed using an unpaired t-test and found to be significantly different (P=0.0131). **(B)** Screening biofilm formation based on the 19 randomly distributed mutants (original value shown with a red dot) with subsequent verification (black dots). M19_R (turquoise), which represents $M19_{retransformed}$, was not included in the statistical analysis presented here. Mutants were compared to KPC-2 and data were analyzed using one-way ANOVA and Dunnett's multiple comparisons tests. M19 was the only significant mutant and is indicated as follows; ****P<0.0001.

To exclude that the observed increase in biofilm formation was due to chromosomal mutations, the M19 vector was isolated and retransformed into *V. cholerae* (named $M19_{retransformed}$). Pellicle formation after 24 hours and antimicrobial susceptibility towards ampicillin were evaluated both before and after retransformation for comparison (Table 4.4). After 24 hours, M19 displayed pellicle formation, although not extending the entire air-liquid interface, whereas no pellicle formation was seen in $M19_{retransformed}$ (Appendix C). Biofilm quantification of $M19_{retransformed}$ demonstrated a >1.2-fold decrease compared to M19 (Figure

4.7B). Nonetheless, the increased biofilm formation compared to KPC-2 remained significant after retransformation (unpaired t-test, P=0.0016). However, subsequent sequence results revealed that $M19_{retransformed}$ was KPC-2 wild type, implying that the observed compensated biofilm phenotype was due to mutations on the vector backbone.

Table 4.4. Resulting static biofilm formation of M19 and $M19_{retransformed}$ after 24 hours. KPC-2 is included for comparison. MIC susceptibility profiles towards ampicillin. Pellicle phenotype after 24 hours is scored as yes or no. For graphical documentation of pellicles see Appendix C.

Strain	OD_{595}	Log_{10} OD_{595}	Log_{10} OD_{595} SEM	MIC Ampicillin (mg/L)	Pellicle phenotype
KPC-2	0.327	-0.486	± 0.040	>256	No
M19	0.725	-0.140	± 0.099	>256	Yes
$M19_{retransformed}$	0.579	-0.237	± 0.096	>256	No

4.3.2 Mutations in KPC-2 restore biofilm formation

Despite the difference in biofilm formation between KPC-2 and the KPC-2 mutant library, the screening efforts described under 4.3.1 did not result in the discovery of any KPC-2 mutants that increased biofilm formation. This prompted me to set up a biofilm selection assay. I hypothesized that this selection scheme potentially could enrich for KPC-2 mutants with increased biofilm-forming capacity more effectively. For this, the ability of strains producing KPC-2 and KPC-2:library to form pellicles in comparison to pCTRL and wtVC was investigated after 24 and 48 hours of static incubation. After 24 hours, wtVC, pCTRL, and KPC-2:library formed pellicles, although to various extents (Figure 4.8). Pellicles of wtVC and KPC-2:library were more mature compared to pCTRL. As expected, KPC-2 displayed no pellicle formation after 24 hours. While all four strains displayed pellicle formation after 48 hours of incubation, there was still a substantial qualitative difference between the pellicle biofilms (Figure 4.8). The difference between KPC-2 and the corresponding KPC-2:library was especially striking. Biofilm pellicles formed by the KPC-2:library strain had more notable structures and greater structural integrity compared to KPC-2.

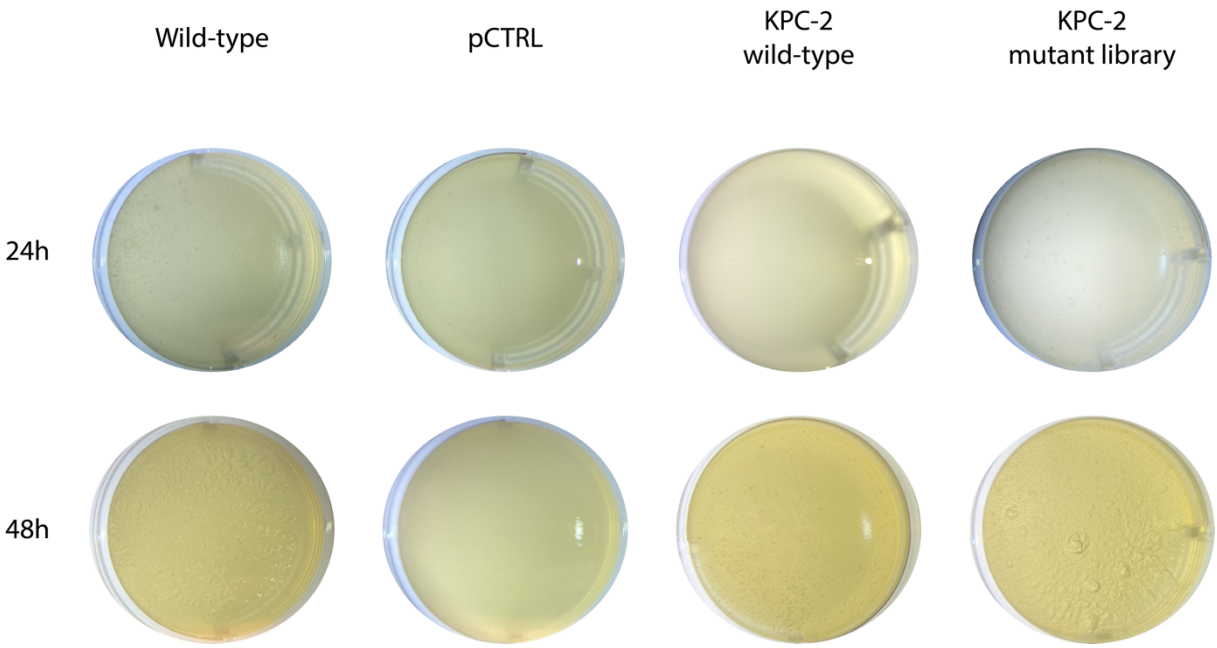

Figure 4.8. Morphology of biofilm pellicles of KPC-2, KPC-2:library, wtVC, and pCTRL after 24 and 48 hours of static incubation at 37°C.

Due to the observed differences between the biofilm pellicles of KPC-2- and KPC-2:library, it was hypothesized that the KPC-2:library could harbor mutants with increased biofilm-forming capacities. It is possible to actively select for biofilm formation in *V. cholerae* and other Gram-negative bacteria by the isolation and propagation of biofilm-embedded bacteria. To limit the number of potentially confounding chromosomal mutations, a one-step selection procedure was employed to enrich for potential KPC-2 mutants growing in the formed pellicles. Pellicle formation was identified visually, and morphology was documented after 24 and 48 hours. After 48 hours, KPC-2:library-pellicles were harvested and broken down and resuspended in PBS. Single-evolved clones were obtained by streaking the resuspended broken-down pellicle populations on LB plates followed by picking of single colonies. The clones' biofilm formation capacities were investigated by measuring the biofilm formation with the CV assay. In addition, pellicle formation and its morphology were also documented.

Seven random single-evolved clones were isolated and sent to sequencing. This revealed that four of the seven clones were wtKPC-2, whereas three clones contained changes in their amino acid sequence (Figure 4.9). One of the mutants had three single amino acid substitutions (N136D/M152I/L167P) as well as a deletion of two nucleotides in nucleotide position 40-41. The deletion led to the introduction of two major changes. First, a premature

stop codon was introduced which resulted in the removal of the first 33 amino acids including the signal peptide. Second, this deletion shifted the DNA translation to an alternative and shorter in-frame reading frame of KPC-2 beginning from amino acid number 49. The remaining two colonies displayed single mutants of KPC-2 harboring the exact same amino acid change (N136K). The triple mutant (named $C2_{selected}$) and one of the identical single mutants (named $C3_{selected}$) were isolated for further investigation.

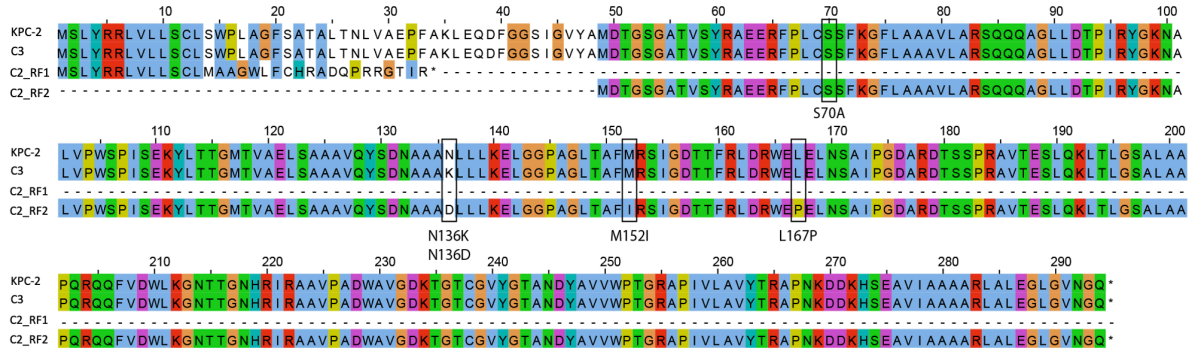

Figure 4.9. Multiple sequence alignment of KPC-2, $C2_{selected}$, and $C3_{selected}$ using Clustal omega (47). Both reading frames of $C2_{selected}$ are presented; the first reading frame (C2_RF1) includes amino acids 1-33. The nucleotide deletions in nucleotide positions 40 and 41 (amino acid position 14) led to a frameshift which subsequently introduced a premature stop codon. The second reading frame (C2_RF2) is introduced by a new start codon and includes amino acids 49-294. Amino acid substitutions found in $C2_{recloned}$ (N136D/M152I/L167P) and $C3_{recloned}$ (N136K), and the active-site Ser70, are shown in brackets at their respective positions. The colored residues are indicated as follows; Blue: hydrophobic. Red: positive charge. Magenta: negative charge. Green: polar. Orange: glycines. Yellow: prolines. Cyan: aromatic. White: unconserved.

The isolated *V. cholerae* strains harboring the triple-mutant ($C2_{selected}$) and the single-mutant ($C3_{selected}$) were subjected to biofilm quantification assay directly after biofilm selection (Table 4.5 and Figure 4.10). This demonstrated that $C2_{selected}$ and $C3_{selected}$ produced more biofilm compared to both KPC-2 and pCTRL. In detail, both $C2_{selected}$ and $C3_{selected}$ produced significantly more biofilm compared to KPC-2 (one-way ANOVA, $P<0.0001$ for both. Figure 4.10A). Compared to pCTRL, $C2_{selected}$ displayed significantly increased biofilm formation

(one-way ANOVA, P=0.0047. Figure 4.10B). $C3_{selected}$ displayed increased biofilm formation relative to pCTRL as well, however, not significantly (P=0.4116).

To exclude confounding chromosomal mutations or mutations in the vector backbone, the bla_{KPC-2} gene from $C2_{selected}$ and $C3_{selected}$ was re-cloned into an isogenic vector backbone and transformed into an isogenic *V. cholerae* (named $C2_{re-cloned}$ and $C3_{re-cloned}$). Thus, making it possible to isolate the biofilm effects of the identified KPC-2 mutants. Following re-cloning, a decrease in biofilm formation by ~2-fold and ~2.6-fold of $C2_{re-cloned}$ and $C3_{re-cloned}$ was observed. Thereby, confirming that the strong biofilm selection pressure in addition selected for confounding mutations outside of bla_{KPC-2} (Table 4.5). Nonetheless, both $C2_{re-cloned}$ and $C3_{re-cloned}$ still displayed significantly higher biofilm formation relative to KPC-2 (one-way ANOVA, P<0.0001 and P=0.0301 respectively. Figure 4.10A), whereas $C2_{re-cloned}$ even displayed biofilm formation to a similar extent as pCTRL (one-way ANOVA, P=0.9997. Figure 4.10B). Compared to each other, $C2_{re-cloned}$ displayed >1.8-fold higher biofilm formation relative to $C3_{re-cloned}$ (two-tailed t-test, P<0.0001. Figure 4.10C). Their ability to form pellicles after 24 hours agreed with the crystal violet assay as both clones, before and after re-cloning, were able to form pellicles, although the biofilm pellicles formed after re-cloning were weaker compared to before re-cloning (Figure 4.11). These findings indicate that the identified mutations in KPC-2 have a profound effect on the biofilm-forming capacity of *V. cholerae* and compensate for the initial KPC-2-mediated decrease in biofilm formation.

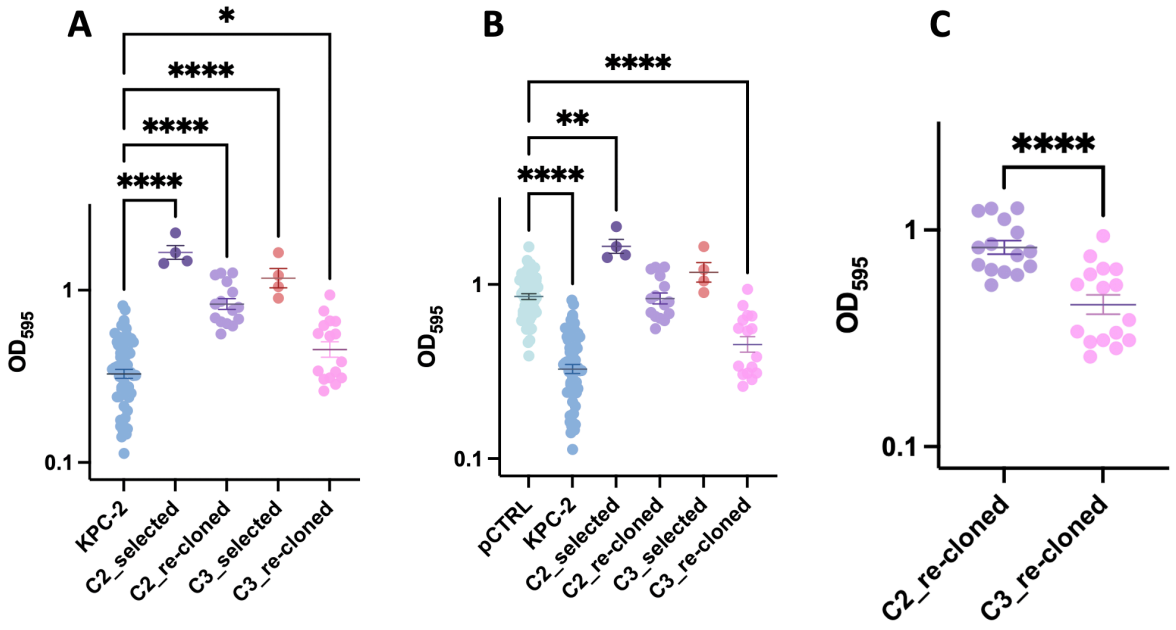

Figure 4.10. Static biofilm formation of C2, C3, KPC-2, and pCTRL after 24 hours of incubation. The strains are presented on the x-axis and OD_{595nm} values are presented on the log y-axis. Each dot represents the OD of a single biological replicate. Bars represent the average, and the error bars represent the standard error of the mean (SEM). Sample size: pCTRL, n=61; KPC-2, n=61; $C2_{selected}$, n=4; $C2_{re\text{-}cloned}$, n=15; $C3_{selected}$, n=4; $C3_{re\text{-}cloned}$, n=16. **(A)** Biofilm formation of $C2_{selected}$, $C2_{re\text{-}cloned}$, $C3_{selected}$, and $C3_{re\text{-}cloned}$ compared to KPC-2. **(B)** Biofilm formation of KPC-2, $C2_{selected}$, $C2_{re\text{-}cloned}$, $C3_{selected}$, and $C3_{re\text{-}cloned}$ compared to pCTRL. **(C)** Biofilm formation of $C2_{re\text{-}cloned}$ and $C3_{re\text{-}cloned}$ compared to each other. Datasets presented in **A** and **B** were analyzed using one-way ANOVA and Dunnett's multiple comparisons tests. Statistical significance is indicated by asterisks as follows: *P=0.0301; **P=0.0047; ****P <0.0001. $C2_{re\text{-}cloned}$ and $C3_{selected}$ were not significantly different relative to pCTRL. Data presented in **C** were analyzed using an unpaired two-tailed t-test. Statistical significance is indicated by asterisks as follows: ****P<0.0001.

Table 4.5. MIC susceptibility profiles towards ampicillin, given as mg/L. Ampicillin MIC test of $C2_{selected}$ and $C3_{selected}$ was not performed. Pellicle phenotype after 24 hours is scored as yes or no.

Strain/ name	Description	OD_{595}	Log_{10} OD_{595}	Log_{10} OD_{595} SEM	Amp MIC	Pellicle phenotype
KPC-2	KPC-2 wild type	0.327	-0.486	± 0.040	>256	No
pCTRL	wtVC carrying pUN	0.853	-0.069	± 0.065	3-4	Yes
$C2_{selection}$	KPC-2: Δ1-48/N136D/ M152I/L167P	1.655	0.219	± 0.307	NT	Yes
$C2_{re\text{-}cloned}$	KPC-2: Δ1-48/N136D/ M152I/L167P	0.831	-0.080	± 0.119	2	Yes
$C3_{selection}$	KPC-2: N136K	1.174	0.070	± 0.307	NT	Yes
$C3_{re\text{-}cloned}$	KPC-2: N136K	0.453	-0.344	± 0.093	24	Yes
$C2_{re\text{-}cloned}$S70A	$C2_{re\text{-}cloned}$: S70A	0.226	-0.645	± 0.038	4	No
KPC-2: S70A	KPC-2: S70A	0.290	-0.537	± 0.067	4	No

NT = not tested

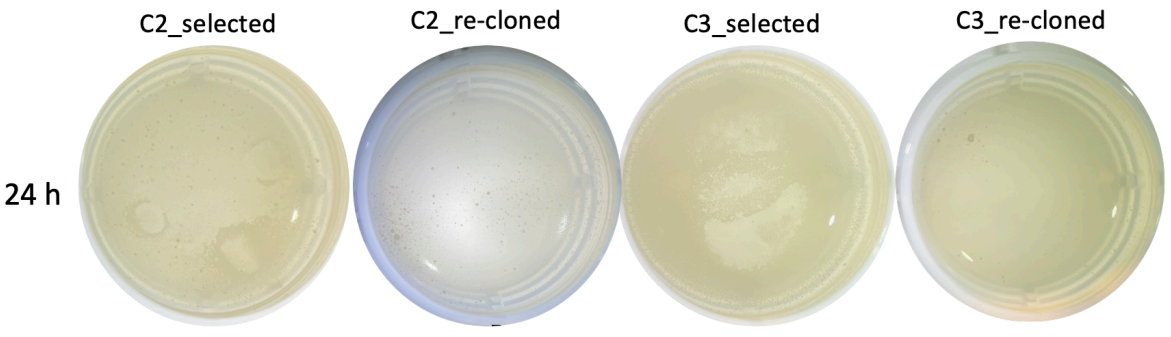

Figure 4.11. Morphology of biofilm pellicles of $C2_{selected}$, $C2_{re\text{-}cloned}$, $C3_{selected}$, and $C3_{re\text{-}cloned}$ after 24 hours of static incubation at 37°C.

4.3.3 Functional and structural role of KPC-2 mutations

The observed changes in biofilm formation in the isolated KPC-2 mutants indicate the importance of these amino acid changes in relation to biofilm formation. Next, I aimed to investigate the functionality of the observed mutants. For this, their biofilm-forming capacity (CV assay and morphology) and their ability to hydrolyze the β-lactam ampicillin were evaluated and compared to KPC-2 (Table 4.5). To assess the functionality even further, active-site mutations of KPC-2 and $C2_{re\text{-}cloned}$ were constructed. These mutants contain an active-site serine to alanine (S70A) substitution that disrupts β-lactam binding, thereby, abolishing the hydrolytic activity of KPC-2 towards β-lactams. It was hypothesized that the disruption of binding would result in the loss of the function that was gained during selection.

Firstly, antimicrobial susceptibility towards ampicillin was evaluated. Both $C2_{re\text{-}cloned}$ and $C3_{re\text{-}cloned}$ displayed enhanced susceptibility toward ampicillin relative to KPC-2 (Table 4.5). In detail, a >10-fold decrease in MIC was observed for $C3_{re\text{-}cloned}$, whereas $C2_{re\text{-}cloned}$ lowered the MIC 128-fold relative to KPC-2, thus restoring wtVC resistance. Consequently, the binding inefficient mutant $C2_{re\text{-}cloned}$S70A did not display a further reduction in the ampicillin MIC. As expected, the introduction of S70A in KPC-2 resulted in a 64-fold reduction in MIC due to the inability of this mutant to bind β-lactams. The substantial change in ampicillin resistance mediated by $C2_{re\text{-}cloned}$ is likely due to the loss of the signal peptide (as described under 4.3.2). However, the functionality data demonstrate that $C3_{re\text{-}cloned}$ maintains relatively high resistance towards β-lactams while partly compensating for the reduction in biofilm formation (Figure 4.10).

Next, I assayed the ability of KPC-2:S70A and $C2_{re\text{-}cloned}$S70A to produce biofilms compared to KPC-2 (Table 4.5 and Figure 4.12). Firstly, compared to KPC-2, the production of KPC-2:S70A resulted in a >1.1-fold reduction in biofilm. However, this reduction was not significant (one-way ANOVA, P=0.8924). On the contrary, $C2_{re\text{-}cloned}$S70A yielded a similar biofilm score compared to KPC-2:S70A, and a significant change in biofilm formation compared to KPC-2 (one-way ANOVA, P=0.0428). KPC-2:S70A and $C2_{re\text{-}cloned}$S70A were unfortunately tested with different sample sizes (n=7 and n=11). Thus, the non-significance of KPC-2:S70A *versus* KPC-2 could be a type-2 error and more samples would improve the statical resolution. Interestingly, $C2_{re\text{-}cloned}$S70A caused a dramatic >3.6-fold reduction in biofilm formation compared to $C2_{re\text{-}cloned}$ (one-way ANOVA, P<0.0001, Figure 4.12). This

could indicate that the observed changes in biofilm formation were due to functional effects of the acquired mutations rather than loss of function of KPC-2.

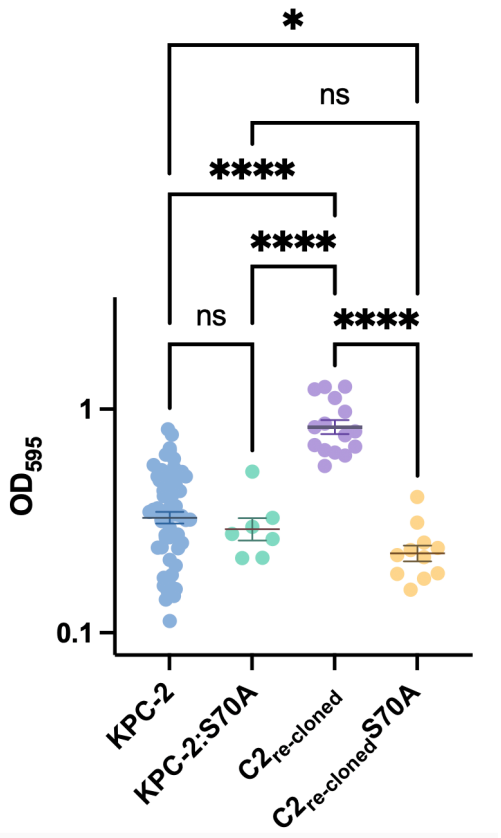

Figure 4.12. Static biofilm formation after 24 hours of KPC-2, KPC-2:S70A, $C2_{re\text{-}cloned}$, and $C2_{re\text{-}cloned}$S70A. The mean of each strain was compared to the mean of every other strain. The strains are presented on the x-axis and OD_{595nm} values are presented on the log y-axis. Each dot represents the OD of a single biological replicate. Bars represent the average and error bars represent the standard error of the mean (SEM). Sample size: KPC-2 n=61; KPC-2:S70A n=7; $C2_{re\text{-}cloned}$ n=15; $C2_{re\text{-}cloned}$S70A n=11. Data were analyzed using one-way ANOVA and Dunnett's multiple comparisons tests. Statistical significance is indicated by asterisks as follows: *P=0.0428; **** P<0.0001; ns = not significant.

In order to better understand the effects of the observed mutations, the amino acid changes observed in $C2_{re\text{-}cloned}$ were plotted onto the structure of KPC-2 covalently bound to a β-lactamase inhibitor (PBP no. 3RXX) (48). The single mutant $C3_{re\text{-}cloned}$ shared a mutation in the same position (N136K) as $C2_{re\text{-}cloned}$ and was therefore not shown separately. Two of the

three mutations (N136D and L167P) are within the active site of KPC-2, and close to amino acids which are considered important for KPC-2 in the hydrolysis of β-lactams (Figure 4.13B). E166 is a key amino acid within KPC-2 and all other class A β-lactamases. This amino acid residue activates the deacylating water which facilitates the termination of the β-lactam from the acyl-enzyme complex. Both N136D and N136K affect the conserved asparagine which interacts with E166 via H-bonds in KPC-2 (Figure 4.13D) (15). In addition, L167P is positioned directly downstream of the E166. Interestingly, N136D and L167P are neighboring amino acids (distance 5 Å) sitting in different loop structures which may indicate that these amino acid changes have a combined effect (Figure 4.13C). The potential effects of M152I remain elusive due to its distance from the active site. In general, this structural investigation indicates that amino acid changes within the active site correlate with increased biofilm formation.

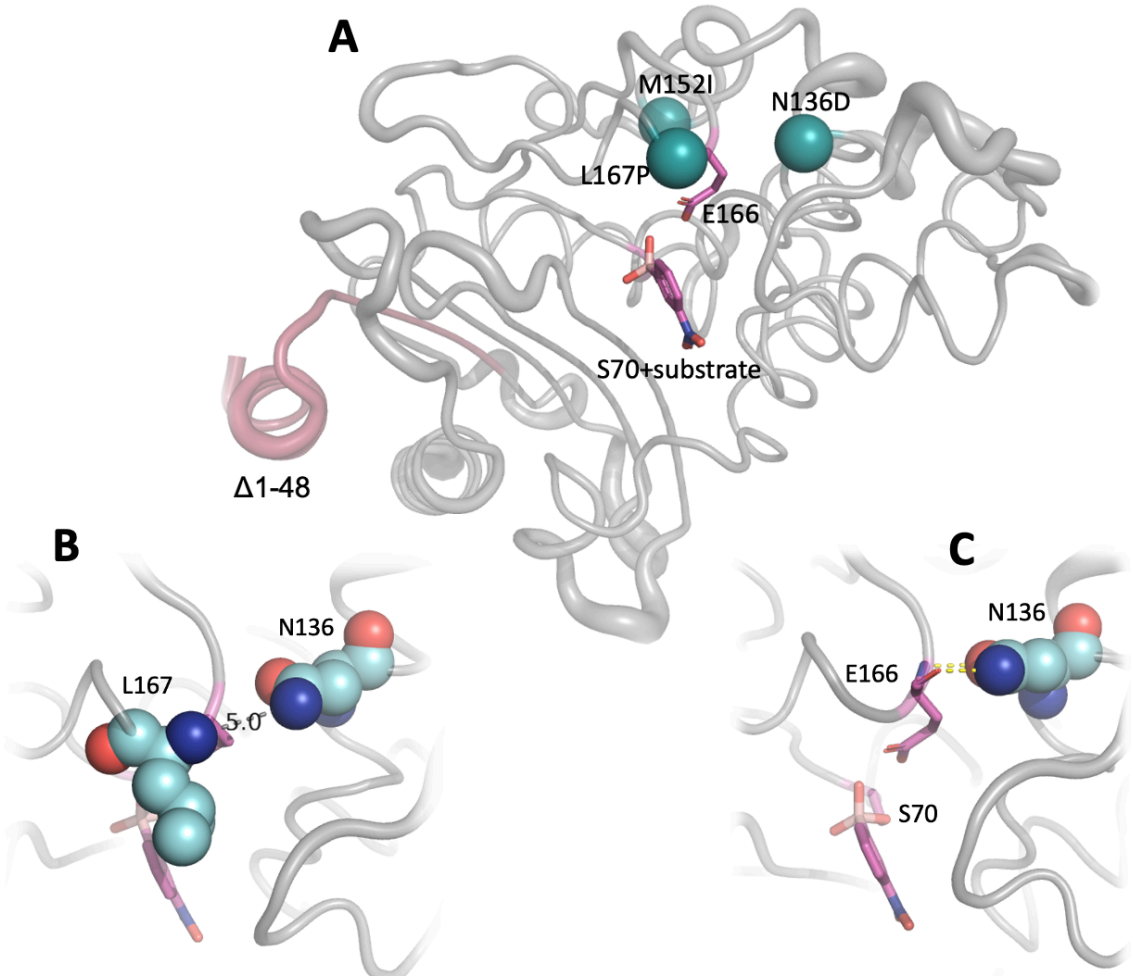

Figure 4.13. KPC-2 active site and mutational influence. S70, E166, and the substrate are colored and shown as sticks. The substrate, a β-lactamase inhibitor, is covalently bound to S70. **(A)** Shows the deletion in $C2_{re\text{-}cloned}$: Δ1-48 (weak red). The three mutations acquired in $C2_{re\text{-}cloned}$ are presented as green spheres. **(B)** The distance (5 Å) between side-chain N in N136 and main-chain N in L167 is shown. **(C)** The two H-bonds between E166 and N136 are shown. The figure above is based on the PBP no. 3RXX and was prepared in Pymol (48).

5 Discussion

The production of β-lactamases is the leading cause of β-lactam resistance in Gram-negative pathogens. β-lactam antibiotics are the most prescribed antibiotics globally and their extensive use is driving the acquisition (e.g., horizontal gene transfer) and evolution of genes encoding for these enzymes. (9, 17, 22, 40). Yet, only a few studies have investigated how the acquisition of these enzymes affects the most common bacterial lifestyle, biofilms (25-27, 49). While these studies showed that the production of β-lactamases can inhibit biofilm formation, they only focused on a limited selection of enzymes (TEM-1, OXA-3, BlaS, AmpC, and TEM-1, SFO-1, OXA-10, and OXA-23) in *E. coli* and *P. aeruginosa* (8, 36). Importantly, none of these studies have investigated how the biofilm lifestyle affects the evolution of β-lactamases. Consequently, the understanding of the relationship between β-lactamases and biofilm formation and vice versa is incomplete. This master project aimed to further elucidate this relationship through two main aims. First, expand the number of investigated β-lactamases per Ambler class and how they affect biofilm formation in *V. cholerae*, and second, investigate how the biofilm lifestyle affects the evolution of β-lactamases.

Biofilm formation assays demonstrated that the expression of almost all β-lactamases, from all Ambler classes reduce the ability of *V. cholerae* to form biofilms (Figure 4.1). This difference in biofilm forming capacity could not be explained by changes in fitness measured as growth (Figure 4.3). Generally, the results obtained in this project agree with previous findings showing that the presence of β-lactamases inhibit biofilm formation also in other species. CMY-2 was the only β-lactamase from class C tested in this study. The study from Gallant *et al.* suggested that biofilm inhibition was restricted to class A and D β-lactamases. (8). Although this study found that the expression of CMY-2 significantly decreased biofilm formation, it was difficult to evaluate whether that was due to growth defects or the expression of $bla_{\text{CMY-2}}$ (Figure 4.3G). However, their study tested only one β-lactamase per Ambler class, and the results obtained in this study show that enzymes belonging to the same Ambler classification, such as VIM-2 and NDM-1, may affect biofilm formation differently (Figure 4.1B). Fernández *et al.* also observed differences within class A β-lactamases in regards to biofilm inhibition (36). Therefore, the observed differences between the studies could be related to which β-lactamases were chosen for investigation. In addition, the biofilm formed by *V. cholerae* is fundamentally different in composition compared to *E. coli* and *P.*

aeruginosa (25). Consequently, observed differences between studies may be due to different model organisms as well. The exact mechanism by which these enzymes inhibit biofilm formation is not yet understood. It has been proposed that these enzymes might interfere with cell wall (PG) remodeling, which manifests as a disruption of the structures necessary for bacterial adhesion which is the initial step in biofilm formation (8). Thus, it is imaginable that genetically diverse β-lactamases may affect different cell wall targets in different bacterial strains. However, data supporting this mechanism remains scarce.

By coupling directed evolution of KPC-2 with biofilm pellicle evolution, it was possible to evolve and isolate strains harboring KPC-2 mutants with increased biofilm formation compared to the wild-type KPC-2 (Figure 4.10). The isolated KPC-2 mutants were re-cloned into an isogenic *V. cholerae* strain background to isolate the biofilm effects of the identified KPC-2 mutants. Comparison of biofilm formation before and after re-cloning demonstrated a decrease in biofilm formation. Indicating that the biofilm evolution co-selected for chromosomal or vector mutations that increase biofilm formation. However, the re-cloned KPC-2 mutants maintained significantly higher biofilm levels compared to KPC-2 (Figure 4.10). This confirms that the active selection for biofilm lifestyle can affect the evolutionary trajectory of β-lactamases. This is further strengthened by the fact that the same mutation was observed in several isolated clones originating from one biofilm pellicle (Figure 4.9).

To assess the functionality of the selected KPC-2 mutants ($C2_{re\text{-}cloned}$ and $C3_{re\text{-}cloned}$), antibiotic susceptibility toward ampicillin (Table 4.5) was determined. Antibiotic susceptibility testing demonstrated that $C2_{re\text{-}cloned}$ and $C3_{re\text{-}cloned}$ had reduced tolerance towards ampicillin compared to KPC-2 (Table 4.5). As expected, due to the loss of the signal peptide, $C2_{re\text{-}cloned}$ exhibited a MIC similar to wtVC and pCTRL. On the contrary, $C3_{re\text{-}cloned}$ still retained significant resistance, which was 6x times higher than wtVC (Table 4.5). Two of the three mutations in $C2_{re\text{-}cloned}$ (and the single mutation in $C3_{re\text{-}cloned}$) are in the active site of KPC-2. It might be that the active site has changed too much for the hydrolysis of β-lactams to efficiently happen, which would explain the reduced MIC (Table 4.5, Figure 4.13). N136 is a conserved residue in class A β-lactamases, which influences the position of the active-site residue E166, essential for substrate deacylation, *via* two H-bonds to main-chain atoms in E166 (50). In both $C2_{re\text{-}cloned}$ and $C3_{re\text{-}cloned}$, the uncharged N136 is substituted with charged amino acids (N136D and N136K) which likely would affect the active site (51). Combined data from susceptibility testing and structural analysis indicate that the selected KPC-2 mutants retained

functionality and that the observed increase in biofilm formation was not due to loss of the enzymatic function.

To further investigate changes in functionality, I constructed binding-deficient KPC-2 mutants (S70A) in the KPC-2 and C2 background. I hypothesized that if the changes in biofilm formation were driven by functional effects in KPC-2, the disruption of binding would affect biofilm levels. Surprisingly, disruption of binding in KPC-2 (KPC-2:S70A) did not significantly affect biofilm formation relative to KPC-2. While this is in agreement with published results on OXA-3 in *P. aeruginosa* and *E. coli* (8), this indicates that the initial reduction in biofilm formation was not related to the presence of a functional KPC-2 (with respect to substrate binding). In contrast, disrupting binding in the $C2_{re\text{-}cloned}$ mutant ($C2_{re\text{-}cloned}$S70A) resulted in a complete loss of the evolved increase in biofilm formation (Figure 4.12). Thus, in the evolved C2-variant, the key active-site residue S70 has seemingly been recruited in the compensation of the initial reduction in biofilm formation. Overall, these results provide further evidence that the evolutionary changes in KPC-2, affecting biofilm levels, are likely due to gain-of-function rather than loss-of-function mutations (impairment of the enzyme).

Introducing a vector control (pCTRL) in wtVC substantially reduced bacterial fitness (growth rate) (Figure 4.3). Further efforts to construct control vectors (pCTRL2 and pCTRL3) as similar to the *bla*-expressing vectors as possible did not mitigate the observed plasmid-mediated reduction in bacterial fitness. At the start of this study, Jaskólska *et al*. described a novel plasmid defense system in *V. cholerae*, which rapidly eliminates commonly used laboratory vectors (including p15a-based vectors) (38). When evaluating the chloramphenicol resistance, LB agar plates *without* chloramphenicol were used to avoid additive effects (Table 4.3, Figure 4.5). In this MIC assay, pCTRL and CMY-2 displayed two inhibition zones, indicating that a fraction of the bacterial population had undergone plasmid loss. This is in line with published data showcasing the fitness cost and instability of common laboratory vectors in *V. cholerae* due to the activation of plasmid defense systems. Due to the fitness cost and stability issues of the control vector, the effect of β-lactamases on biofilm formation should ideally have been studied with chromosomally inserted *bla* genes. However, this was not feasible due to time restrictions. Furthermore, the presented evolutionary study of KPC-2 would be very challenging to perform with only chromosomal mutations.

The reduced vector stability can to some extent explain the differences observed in the strains' fitness for either pCTRL (including pCTRL2/3) and CMY-2, which had substantially longer lag phases compared to the other strains (Figure 4.3). It is unclear why these vectors had such a large effect on fitness compared to the other tested *bla* genes. This could be due to differences in immunogenicity, meaning that pCTRL and CMY-2 somehow to a greater degree activated the plasmid defense systems of *V. cholerae*. Importantly, all other tested β-lactamases had similar growth rates compared to wtVC and did not exhibit stability issues. Therefore, the observed differences in biofilm formation for the tested β-lactamases, and in particular KPC-2, are almost certainly related to the production of the β-lactamases.

I acknowledge the fact that evolution was only performed with one β-lactamase (KPC-2). Ideally, the generality of these findings should have been studied in a broader selection of enzymes, across different Ambler classes. Along these lines, the mutational study to interrogate functional effects in the evolved KPC-2 variants is limited to only KPC-2 and $C2_{re\text{-}cloned}$. To gain better insight into the functional effects of the acquired mutations, a more comprehensive mutational study is needed (e.g., repair deletion in $C2_{re\text{-}cloned}$, introduce deletion in $C3_{re\text{-}cloned}$, and reconstruct individual point mutations identified in $C2_{re\text{-}cloned}$ and $C3_{re\text{-}cloned}$). However, since no data on the evolutionary connection between β-lactamases and biofilm development exist, this study was meant to serve as a first proof of principle. Broader investigations are needed to study the generality of this effect.

Taken together, this study sheds further light on the effect β-lactamases have on biofilm formation. Importantly, this study describes for the first time that β-lactamases and biofilm producing bacteria can stand in an evolutionary relationship. In their natural environment, bacteria are thought to be under selection pressure towards a biofilm lifestyle, which is reflected in the fact that biofilms are the most common bacterial lifestyle (25). Thus, from an ecological point of view, the evolution of these two factors is likely intertwined. Understanding such evolutionary connections, as described here between biofilm and the evolution of $bla_{KPC\text{-}2}$ in *V. cholerae*, is of importance to understanding the spread and evolution of antimicrobial resistance.

References

1. Hutchings MI, Truman AW, Wilkinson B. Antibiotics: past, present and future. Current Opinion in Microbiology. 2019;51:72-80.
2. Adedeji WA. THE TREASURE CALLED ANTIBIOTICS. Ann Ib Postgrad Med. 2016;14(2):56-7.
3. Rosenblatt-Farrell N. The landscape of antibiotic resistance. Environ Health Perspect. 2009;117(6):A244-50.
4. Darby EM, Trampari E, Siasat P, Gaya MS, Alav I, Webber MA, et al. Molecular mechanisms of antibiotic resistance revisited. Nature Reviews Microbiology. 2023;21(5):280-95.
5. Sauvage E, Kerff F, Terrak M, Ayala JA, Charlier P. The penicillin-binding proteins: structure and role in peptidoglycan biosynthesis. FEMS Microbiol Rev. 2008;32(2):234-58.
6. Reygaert WC. An overview of the antimicrobial resistance mechanisms of bacteria. AIMS Microbiol. 2018;4(3):482-501.
7. Bush K, Bradford PA. β-Lactams and β-Lactamase Inhibitors: An Overview. Cold Spring Harb Perspect Med. 2016;6(8).
8. Gallant CV, Daniels C, Leung JM, Ghosh AS, Young KD, Kotra LP, et al. Common β-lactamases inhibit bacterial biofilm formation. Molecular Microbiology. 2005;58(4):1012-24.
9. Cassini A, Högberg LD, Plachouras D, Quattrocchi A, Hoxha A, Simonsen GS, et al. Attributable deaths and disability-adjusted life-years caused by infections with antibiotic-resistant bacteria in the EU and the European Economic Area in 2015: a population-level modelling analysis. The Lancet Infectious Diseases. 2019;19(1):56-66.
10. Bush K. Characterization of β-lactamases. Antimicrobial agents and chemotherapy. 1989;33(3):259-63.
11. Bush K, Jacoby GA. Updated functional classification of β-lactamases. Antimicrob Agents Chemother. 2010;54(3):969-76.
12. Bush K, Jacoby GA, Medeiros AA. A functional classification scheme for β-lactamases and its correlation with molecular structure. Antimicrobial agents and chemotherapy. 1995;39(6):1211-33.
13. Tooke CL, Hinchliffe P, Bragginton EC, Colenso CK, Hirvonen VHA, Takebayashi Y, et al. β-Lactamases and β-Lactamase Inhibitors in the 21st Century. J Mol Biol. 2019;431(18):3472-500.
14. Stojanoski V, Adamski CJ, Hu L, Mehta SC, Sankaran B, Zwart P, et al. Removal of the Side Chain at the Active-Site Serine by a Glycine Substitution Increases the Stability of a Wide Range of Serine β-Lactamases by Relieving Steric Strain. Biochemistry. 2016;55(17):2479-90.
15. Galdadas I, Lovera S, Pérez-Hernández G, Barnes MD, Healy J, Afsharikho H, et al. Defining the architecture of KPC-2 Carbapenemase: identifying allosteric networks to fight antibiotics resistance. Sci Rep. 2018;8(1):12916.
16. Baier F, Tokuriki N. Connectivity between Catalytic Landscapes of the Metallo-β-Lactamase Superfamily. Journal of Molecular Biology. 2014;426(13):2442-56.
17. Bonomo RA. β-Lactamases: A Focus on Current Challenges. Cold Spring Harb Perspect Med. 2017;7(1).
18. Fröhlich C, Chen JZ, Gholipour S, Erdogan AN, Tokuriki N. Evolution of β-lactamases and enzyme promiscuity. Protein Eng Des Sel. 2021;34.
19. Schultsz C, Geerlings S. Plasmid-Mediated Resistance in Enterobacteriaceae. Drugs. 2012;72(1):1-16.

20. Asokan GV, Ramadhan T, Ahmed E, Sanad H. WHO Global Priority Pathogens List: A Bibliometric Analysis of Medline-PubMed for Knowledge Mobilization to Infection Prevention and Control Practices in Bahrain. Oman Med J. 2019;34(3):184-93.
21. Miton CM, Tokuriki N. How mutational epistasis impairs predictability in protein evolution and design. Protein Science. 2016;25(7):1260-72.
22. Bush K. Past and Present Perspectives on β-Lactamases. Antimicrob Agents Chemother. 2018;62(10).
23. Fröhlich C, Sørum V, Tokuriki N, Johnsen PJ, Samuelsen Ø. Evolution of β-lactamase-mediated cefiderocol resistance. J Antimicrob Chemother. 2022;77(9):2429-36.
24. Kaltenbach M, Jackson CJ, Campbell EC, Hollfelder F, Tokuriki N. Reverse evolution leads to genotypic incompatibility despite functional and active site convergence. eLife. 2015;4:e06492.
25. Flemming H-C, Wingender J, Szewzyk U, Steinberg P, Rice SA, Kjelleberg S. Biofilms: an emergent form of bacterial life. Nature Reviews Microbiology. 2016;14(9):563-75.
26. Conner JG, Teschler JK, Jones CJ, Yildiz FH. Staying Alive: *Vibrio cholerae*'s Cycle of Environmental Survival, Transmission, and Dissemination. Microbiology Spectrum. 2016;4(2):4.2.02.
27. Ciofu O, Moser C, Jensen PØ, Høiby N. Tolerance and resistance of microbial biofilms. Nature Reviews Microbiology. 2022;20(10):621-35.
28. Teschler JK, Nadell CD, Drescher K, Yildiz FH. Mechanisms Underlying *Vibrio cholerae* Biofilm Formation and Dispersion. Annual Review of Microbiology. 2022;76(1):503-32.
29. Kovács ÁT, Dragoš A. Evolved Biofilm: Review on the Experimental Evolution Studies of *Bacillus subtilis* Pellicles. Journal of Molecular Biology. 2019;431(23):4749-59.
30. Traverse CC, Mayo-Smith LM, Poltak SR, Cooper VS. Tangled bank of experimentally evolved *Burkholderia* biofilms reflects selection during chronic infections. Proceedings of the National Academy of Sciences. 2013;110(3):E250-E9.
31. Malone JG. Role of small colony variants in persistence of *Pseudomonas aeruginosa* infections in cystic fibrosis lungs. Infect Drug Resist. 2015;8:237-47.
32. Harris JB, LaRocque RC, Qadri F, Ryan ET, Calderwood SB. Cholera. Lancet. 2012;379(9835):2466-76.
33. Weil AA, Harris JB. Chapter 60 - *Vibrio cholerae.* In: Tang Y-W, Sussman M, Liu D, Poxton I, Schwartzman J, editors. Molecular Medical Microbiology (Second Edition). Boston: Academic Press; 2015. p. 1079-98.
34. Ganguly NK, Kaur T. Mechanism of action of cholera toxin & other toxins. Indian J Med Res. 1996;104:28-37.
35. Teschler JK, Zamorano-Sánchez D, Utada AS, Warner CJA, Wong GCL, Linington RG, et al. Living in the matrix: assembly and control of *Vibrio cholerae* biofilms. Nature Reviews Microbiology. 2015;13(5):255-68.
36. Fernández A, Pérez A, Ayala JA, Mallo S, Rumbo-Feal S, Tomás M, et al. Expression of OXA-Type and SFO-1 β-Lactamases Induces Changes in Peptidoglycan Composition and Affects Bacterial Fitness. Antimicrobial Agents and Chemotherapy. 2012;56(4):1877-84.
37. Thelin KH, Taylor RK. Toxin-coregulated pilus, but not mannose-sensitive hemagglutinin, is required for colonization by *Vibrio cholerae* O1 El Tor biotype and O139 strains. Infection and Immunity. 1996;64(7):2853-6.
38. Jaskólska M, Adams DW, Blokesch M. Two defence systems eliminate plasmids from seventh pandemic *Vibrio cholerae.* Nature. 2022;604(7905):323-9.
39. Preston KE, Hitchcock SA, Aziz AY, Tine JA. The complete nucleotide sequence of the multi-drug resistance-encoding IncL/M plasmid pACM1. Plasmid. 2014;76:54-65.

40. Fröhlich C, Gama JA, Harms K, Hirvonen VHA, Lund BA, Kamp MWvd, et al. Cryptic β-Lactamase Evolution Is Driven by Low β-Lactam Concentrations. mSphere. 2021;6(2):e00108-21.
41. Di Luca MC, Sørum V, Starikova I, Kloos J, Hülter N, Naseer U, et al. Low biological cost of carbapenemase-encoding plasmids following transfer from *Klebsiella pneumoniae* to *Escherichia coli*. J Antimicrob Chemother. 2017;72(1):85-9.
42. Poirel L, Naas T, Nicolas D, Collet L, Bellais S, Cavallo JD, et al. Characterization of VIM-2, a carbapenem-hydrolyzing metallo-β-lactamase and its plasmid- and integron-borne gene from a *Pseudomonas aeruginosa* clinical isolate in France. Antimicrob Agents Chemother. 2000;44(4):891-7.
43. Samuelsen Ø, Naseer U, Karah N, Lindemann PC, Kanestrøm A, Leegaard TM, et al. Identification of Enterobacteriaceae isolates with OXA-48 and coproduction of OXA-181 and NDM-1 in Norway. Journal of Antimicrobial Chemotherapy. 2013;68(7):1682-5.
44. Poirel L, Castanheira M, Carrër A, Rodriguez CP, Jones RN, Smayevsky J, et al. OXA-163, an OXA-48-related class D β-lactamase with extended activity toward expanded-spectrum cephalosporins. Antimicrob Agents Chemother. 2011;55(6):2546-51.
45. Kanungo S, Azman AS, Ramamurthy T, Deen J, Dutta S. Cholera. The Lancet. 2022;399(10333):1429-40.
46. The European Committee on Antimicrobial Susceptibility Testing. Breakpoint tables for interpretation of MICs and zone diameters. Version 13.0 2023 [Available from: http://www.eucast.org/clinical_breakpoints/.
47. Sievers F, Higgins DG. Clustal Omega, accurate alignment of very large numbers of sequences. Methods Mol Biol. 2014;1079:105-16.
48. Ke W, Bethel CR, Papp-Wallace KM, Pagadala SRR, Nottingham M, Fernandez D, et al. Crystal Structures of KPC-2 β-Lactamase in Complex with 3-Nitrophenyl Boronic Acid and the Penam Sulfone PSR-3-226. Antimicrobial Agents and Chemotherapy. 2012;56(5):2713-8.
49. Silva AJ, Benitez JA. *Vibrio cholerae* Biofilms and Cholera Pathogenesis. PLOS Neglected Tropical Diseases. 2016;10(2):e0004330.
50. Banerjee S, Shigematsu N, Pannell LK, Ruvinov S, Orban J, Schwarz F, et al. Probing the non-proline cis peptide bond in β-lactamase from *Staphylococcus aureus* PC1 by the replacement Asn136 --> Ala. Biochemistry. 1997;36(36):10857-66.
51. Chikunova A, Ubbink M. The roles of highly conserved, non-catalytic residues in class A β-lactamases. Protein Sci. 2022;31(6):e4328.

Appendices

Appendix A: Strains and primers used in this study

Table A1. Strains used and constructed in this study. * = constructed by Rebekka Rolfsnes

Strain/name	Species	Description	Reference
wtVC	*V. cholerae*	wtVC (C6706 El Tor biotype Inaba)	(37)
pCTRL	*V. cholerae*	wtVC carrying pUN	This study*
pCTRL2	*V. cholerae*	wtVC carrying pUN: Δ promotor	This study
pCTRL3	*V. cholerae*	wtVC carrying pUN-bla_{KPC-2}(inactive promotor)	This study
KPC-2	*V. cholerae*	wtVC carrying pUN-bla_{KPC-2}	This study
TEM-1	*V. cholerae*	wtVC carrying pUN-bla_{TEM-1}	This study
CTX-M-15	*V. cholerae*	wtVC carrying pUN-$bla_{CTX-M-15}$	This study
NDM-1	*V. cholerae*	wtVC carrying pUN-bla_{NDM-1}	This study
VIM-2	*V. cholerae*	wtVC carrying pUN-bla_{VIM-2}	This study
CMY-2	*V. cholerae*	wtVC carrying pUN-bla_{CMY-2}	This study
OXA-48	*V. cholerae*	wtVC carrying pUN-bla_{OXA-48}	This study
OXA-163	*V. cholerae*	wtVC carrying pUN-$bla_{OXA-163}$	This study
KPC-2:library	*V. cholerae*	wtVC carrying mutational library of pUN-bla_{KPC-2}	This study
M19	*V. cholerae*	wtVC carrying pUN-bla_{KPC-2}	This study
$M19_{retransformed}$	*V. cholerae*	wtVC carrying pUN-bla_{KPC-2}	This study
KPC-2:S70A	*V. cholerae*	wtVC carrying pUN-$bla_{KPC-2:S70A}$	This study
$C2_{selected}$	*V. cholerae*	wtVC carrying pUN-$bla_{KPC-2:Δ1-48/N136D/M152I/L167P}$	This study
$C2_{re-cloned}$	*V. cholerae*	wtVC carrying pUN-$bla_{KPC-2:Δ1-48/N136D/M152I/L167P}$	This study
$C2_{re-cloned}$S70A	*V. cholerae*	wtVC carrying pUN-$bla_{KPC-2:Δ1-48/N136D/M152I/L167P/S70A}$	This study
$C3_{selected}$	*V. cholerae*	wtVC carrying pUN-$bla_{KPC-2:N136K}$	This study
$C3_{re-cloned}$	*V. cholerae*	wtVC carrying pUN-$bla_{KPC-2:N136K}$	This study
MP 21-05	*E. coli*	*E. coli* E. cloni® 10G	Lucigen
MP 21-05 pUN	*E. coli*	MP 21-05 carrying pUN	(40)
MP 24-45	*E. coli*	MP 21-05 carrying mutational library of pUN-bla_{KPC-2}	(23)
MP 24-44	*E. coli*	MP 21-05 carrying pUN-bla_{KPC-2}	(23)
MP-TEM-1		MP 21-05 carrying pUN-bla_{TEM-1}	This study*
MP 24-80	*E. coli*	MP 21-05 carrying pUN-$bla_{CTX-M-15}$	(23)
MP 24-81	*E. coli*	MP 21-05 carrying pUN-bla_{NDM-1}	(23)
MP-VIM-2		MP 21-05 carrying pUN-bla_{VIM-2}	This study*
MP 12-69	*E. coli*	MP 21-05 carrying pUN-bla_{CMY-2}	(23)
MP 21-02	*E. coli*	MP 21-05 carrying pUN-bla_{OXA-48}	(23)
MP-OXA-163		MP 21-05 carrying pUN-$bla_{OXA-163}$	This study*

Table A2. Primers used and designed in this study. * = designed by my supervisors.

No.	5' – 3'	Reference
P3	GCTTTCCCATGGATGTTTTTCCTCCTTATGTTAAGCTTACTCAG	(23)
P4	GCTT CTCGAG AAGTGGTTAGCGCGTATTTGTG	(23)
P7	GATTACGCGCAGACCAAAACG	(23)
P8	CCTATTTCCCTAAAGGGTTTATTGAGAATATG	(23)
P115	TTTTT GCTCTTC TGTGC GCG TCA TTCAAGGGCTTTCTTGC	This study*
P108	TTTTT GCTCTTC GCACA GTGGGAAGCGCTCC	This study*
P112F	TTTTT GCTCTTC cccat acga aaaaaa cagatatttatga tttttt aac	This study*
P113R	TTTTT GCTCTTC atggg gctgacttcaggtg	This study*

Appendix B: Biofilm quantification by CV staining

Table B1. Biofilm quantification results after 24 hours of static incubation of wtVC, pCTRL, and all 8 β-lactamases included in this thesis. OD_{595} values represent the mean of the sample size (N). The OD values presented here, are multiplied by a factor of 0.6, as mentioned in Chapter 3.5.

Species	**Strain/ β-lactamase**	**OD_{595}**	**Log_{10} OD_{595}**	**Log_{10} OD_{595} SEM**	**Sample size N**
V. cholerae	wtVC	0.795	-0.099	0.041	10
V. cholerae	pCTRL	0.454	-0.343	0.037	77
V. cholerae	KPC-2	0.176	-0.755	0.020	56
V. cholerae	TEM-1	0.223	-0.652	0.049	12
V. cholerae	CTX-M-15	0.206	-0.686	0.056	8
V. cholerae	NDM-1	0.398	-0.400	0.025	4
V. cholerae	VIM-2	0.187	-0.727	0.017	8
V. cholerae	CMY-2	0.210	-0.677	0.017	8
V. cholerae	OXA-48	0.216	-0.665	0.032	16
V. cholerae	OXA-163	0.242	-0.617	0.053	12

Appendix C: Morphology of biofilm pellicle of KPC-2, M19, and $M19_{retransformed}$.

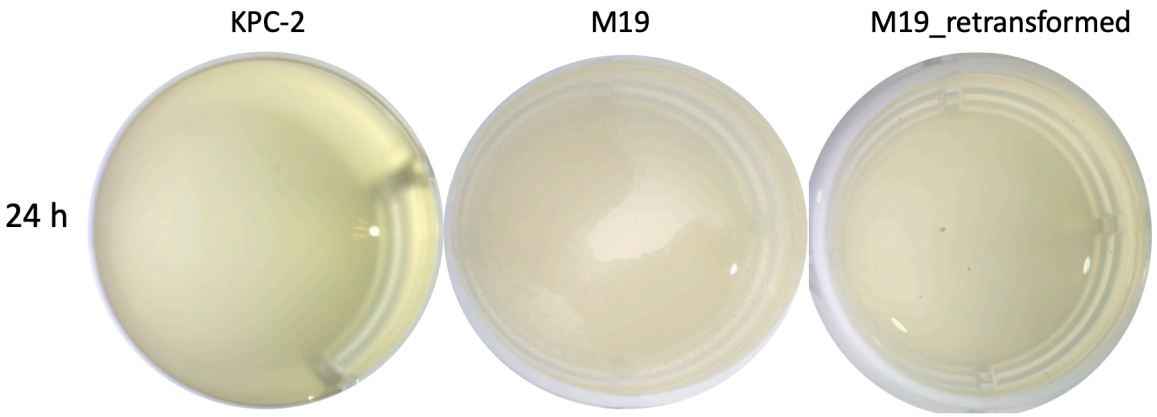

Figure: Morphology of biofilm pellicles of KPC-2, M19, and $M19_{retransformed}$ after 24 hours of static incubation at 37°C.